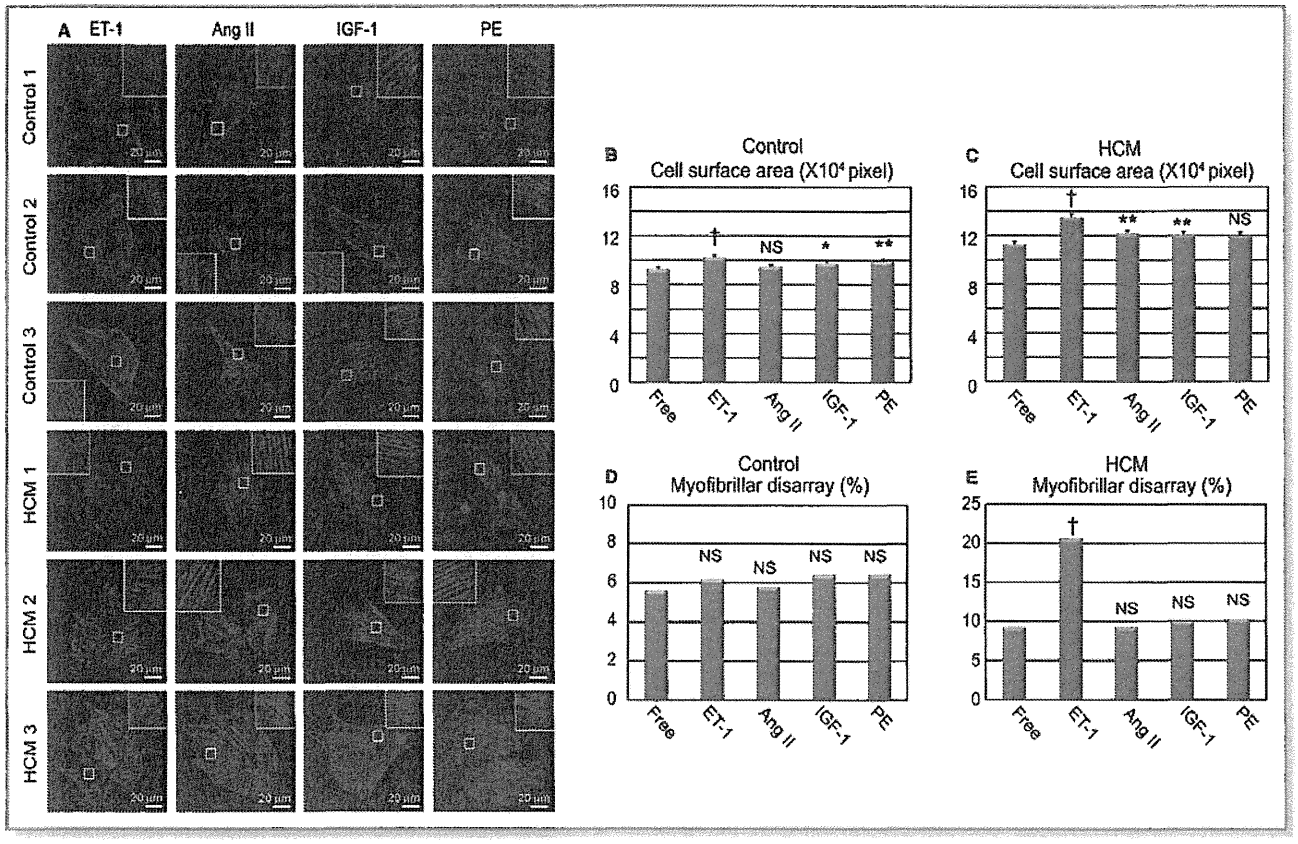

Figure 9. ET-1 augments pathological features in HCM iPSC-derived cardiomyocytes. A, Immunostaining for cardiac troponin-T (cTnT) of the single cardiomyocytes derived from each control and HCM iPSC. The single cardiomyocytes at 60 days were cultured for 7 days with ET-1, Ang II, IGF-1, or PE. B and C, Cell surface areas of 788 to 819 randomly chosen cTnT-positive cardiomyocytes in each group and condition were measured. The single cardiomyocytes were cultured for 7 days with ET-1, Ang II, IGF-1, or PE (1-way ANOVA with Steel's multiple comparison post-test). D and E. The percentages of cardiomyocytes with myofibrillar disarray were assessed by immunostaining for cTnT. N=844 to 995. *P<0.05, **P<0.01, †P<0.0001 vs free condition (χ^2 test). Ang II indicates angiotensin II; ET-1, endothelin-1; HCM, hypertrophic cardiomyopathy; IGF-1, insulin-like growth factor-1; iPSC, induced pluripotent stem cell; PE, phenylephrine.

and HCM iPSC-derived cardiomyocytes. There were no significant differences in extracellular signal-regulated kinase and c-Jun N-terminal kinase activation by ET-1 stimulation between control and HCM (data not shown).

The ET-1–ETA Axis has a Pivotal Role in Pathological Deterioration in HCM iPSC-Derived Cardiomyocytes

To further investigate the potential therapeutic strategy of blocking ET-1 signaling for disease prevention and regression, we examined the effects of ETA-b (BQ-123) and ETB-b (BQ-788) on the HCM iPSC-derived cardiomyocytes, based on the cell surface area and the incidence of myofibrillar disarray. We added ETA-b and ETB-b for 7 days with ET-1 to the HCM iPSC-derived cardiomyocytes (Figure 13A). ETA-b apparently blocked the ET-1–induced cardiomyocyte hypertrophy, while no antihypertrophic effect was observed with ETB-b (Figure 13A and 13B). In addition, coadministration of ETA-b and ETB-b attenuated the increased cell surface area induced by ET-1. Without ET-1, coadministration of ETA-b and ETB-b did not significantly affect cell surface area of the HCM iPSC-derived cardiomyocytes. Moreover, ETA-b, but not ETB-b, significantly decreased the incidence of ET-1–induced myofibrillar disarray in the HCM iPSC-derived cardiomyocytes (Figure 13A and 13C). Electron microscopy of beating EBs treated with ET-1 for 7 days also revealed attenuation of the increased myofibrillar disarray with ETA-b, but not ETB-b (Figure 13D and 13E). Although some previous reports showed that ETA-b and ETB-b both have antagonizing effects on ET-1 in various tissues,[26] ETB-b showed no such action on the ET-1–induced hypertrophy and incidence of myofibrillar disarray in the HCM iPSC-derived cardiomyocytes. These data suggest that ETA-b might have a preventive effect on disease manifestation in HCM iPSC-derived cardiomyocytes. Next, we examined the effect of ET-1 blockers on NFATc4 nuclear

Downloaded from http://jaha.ahajournals.org/ at KEIO UNIVIVERSITY on February 15, 2015

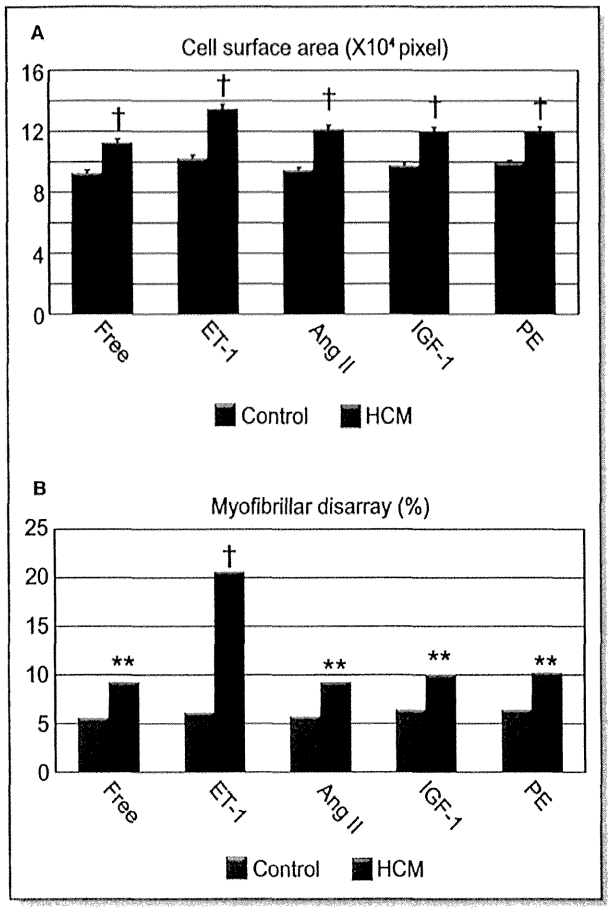

Figure 10. Increased pathological features in HCM iPSC-derived cardiomyocytes. A, The single cardiomyocytes at 60 days after differentiation were cultured for 7 days with ET-1, Ang II, IGF-1, or PE. Cell surface areas of cTnT-positive cardiomyocytes were measured. N=788 to 819. †P<0.0001 vs control in the same condition (Mann–Whitney U test). B, The percentages of cardiomyocytes with myofibrillar disarray were assessed by immunostaining for cardiac troponin-T. N=844 to 995. **P<0.01, †P<0.0001 vs control in the same condition (χ^2 test). Ang II indicates angiotensin II; cTnT, cardiac troponin-T; ET-1, endothelin-1; HCM, hypertrophic cardiomyopathy; IGF-1, insulin-like growth factor-1; iPSC, induced pluripotent stem cell; PE, phenylephrine.

translocation in HCM iPSC-derived cardiomyocytes. ETA-b, but not ETB-b, significantly decreased ET-1–induced NFATc4 nuclear translocation in the HCM iPSC-derived cardiomyocytes (Figure 13F and 13G).

Next, we examined the effect of ETA-b on regressing the HCM pathological phenotype (Figure 14A). Interestingly, ET-1 treatment of these cells during either the first or second 7-day period significantly increased both cell surface area and the incidence of myofibrillar disarray at 14 days (Figure 14B through 14D: ET-1-Free, Free-ET-1). These data suggest that once cardiomyocytes acquire the HCM pathological state, it is difficult to spontaneously attenuate the phenotype. ETA-b administration during the latter 7 days significantly reduced the cell surface area and the incidence of myofibrillar disarray in the ET-1–treated HCM iPSC-derived cardiomyocytes (Figure 14B through 14D: ET-1-ETA-b). These data implicate the importance of ET-1 and the ETA pathway in the pathological progression and regression of HCM.

ET-1 Has a Pivotal Role in Myofibrillar Disarray in Heterozygous *Mybpc3*-Targeted Knock-in Mouse Myocytes

We showed that ET-1 induced myofibrillar disarray in the HCM iPSC-derived cardiomyocytes. We then examined whether this phenotype is reproduced in a well-characterized mouse model of HCM. We chose the heterozygous *Mybpc3*-targeted knock-in mice (HET),[16] which mimic the genetic situation of HCM patients, such as the present HCM 3. HET mice developed diastolic dysfunction but no cardiac hypertrophy.[27] Interestingly, however, engineered heart tissue derived from neonatal HET mice exhibited accumulation of hypertrophic markers, suggesting that culture conditions could reveal hypertrophy in *Mybpc3*-carrier mice. Cardiomyocytes were isolated from HET and wild-type (WT) neonatal mice and cultured for 72 hours; serum was then removed for 12 hours, and thereafter cells were stimulated by either ET-1 or control for 48 hours. We then measured cell surface area and myofibrillar disarray after immunostaining for α-actinin and cMyBP-C (Figure 15A and 15B). In basal conditions, HET cardiomyocytes were larger than those of WT but did not exhibit higher incidence of myofibrillar disarray than WT cardiomyocytes (Figure 15C and 15D: Control). ET-1 induced a similar extent of cardiomyocyte hypertrophy in WT and HET (Figure 15C). On the other hand, whereas ET-1 had no effect on the myofibrillar disarray in WT cells, it markedly increased the incidence of myofibrillar disarray in HET (Figure 15D). In baseline conditions, mRNA levels for *actin, alpha 1, skeletal muscle* (*Acta1*), *natriuretic peptide type A* (*Nppa*), and *natriuretic peptide type B* (*Nppb*) were all higher in HET than in WT cells. ET-1 increased all of them in both groups and particularly *Nppb* mRNA levels in HET cardiomyocytes (Figure 15E through 15G). These data suggest that ET-1 induces pathological cardiac phenotypes in the HCM model.

Contraction Variability Is Captured by Motion Vector Analysis in Single Beating Cardiomyocytes Derived From iPSCs

We showed herein that myofibrillar disarray increased by ET-1 and decreased by ETA-b in HCM iPSC-derived cardiomyocytes. To elucidate whether myofibrillar disarray in beating human cardiomyocytes can affect physiological properties, we last analyzed the contractile dynamics of the self-beating iPSC-derived single cardiomyocytes in terms of contractile

Downloaded from http://jaha.ahajournals.org/ at KEIO UNIVIVERSITY on February 15, 2015

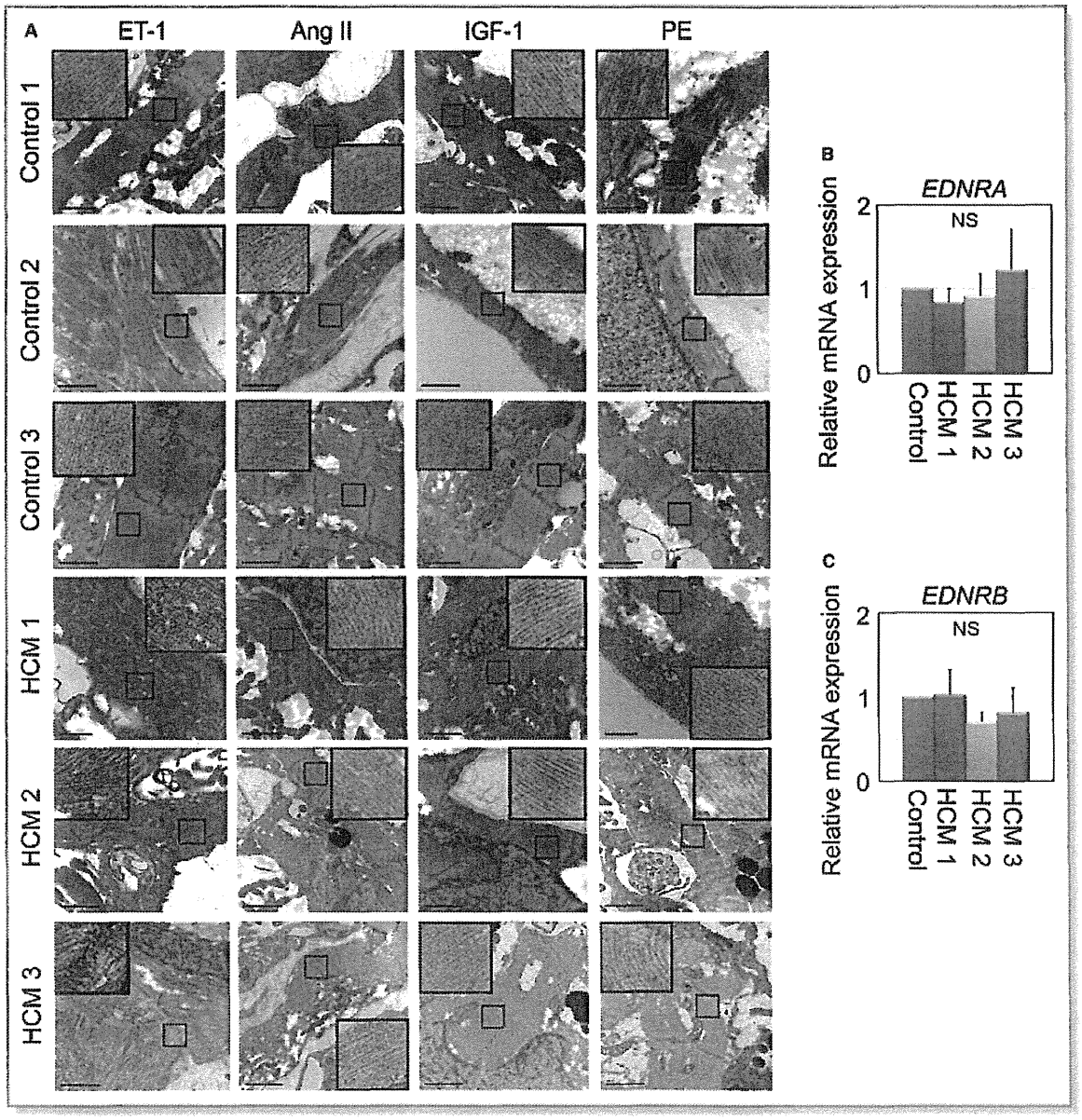

Figure 11. ET-1 augments myofibrillar disarray in HCM iPSC-derived cardiomyocytes. A, Electron microscopic observation of beating EBs at 60 days, which were cultured with ET-1, Ang II, IGF-1, or PE for 7 days. Scale bars, 1 μm. B and C, Relative gene expression of *EDNRA* and *EDNRB* in beating EBs at 30 days, normalized against *TNNT2*. N=3 (Control=3, HCM 1=3, HCM 1=3, HCM 3=3) (Kruskal–Wallis test). Ang II indicates angiotensin II; EBs, embryoid bodies; EDNRA, endothelin receptor type A; ET-1, endothelin-1; HCM, hypertrophic cardiomyopathy; IGF-1, insulin-like growth factor-1; iPSC, induced pluripotent stem cell; PE, phenylephrine.

direction, using a high-speed video imaging and analysis system.[12] This system can evaluate contractile direction of every moving spot detected in a spontaneously beating cardiomyocyte and produce an index of contractile dispersion (Figure 16). To analyze variability in the contractile direction, iPSC-derived cardiomyocytes were cultured under adherent culture conditions for 24 hours after beating EBs were dissociated (0 hours) and treated with ET-1 in the absence or presence of ETA-b or ETB-b for 24 or 48 hours. Motion vector pictures (Vector) showed the captured motion direction and distance at each point in each single beating cardiomyocyte, and histograms indicated the corresponding point frequencies at a range of angles (0° to 180°; Figure 17A). We compared the variation in the SD scores of the histogram between control and HCM iPSC-derived cardiomyocytes. Before ET-1 administration (Free), the histograms of control

Downloaded from http://jaha.ahajournals.org/ at KEIO UNIVIVERSITY on February 15, 2015

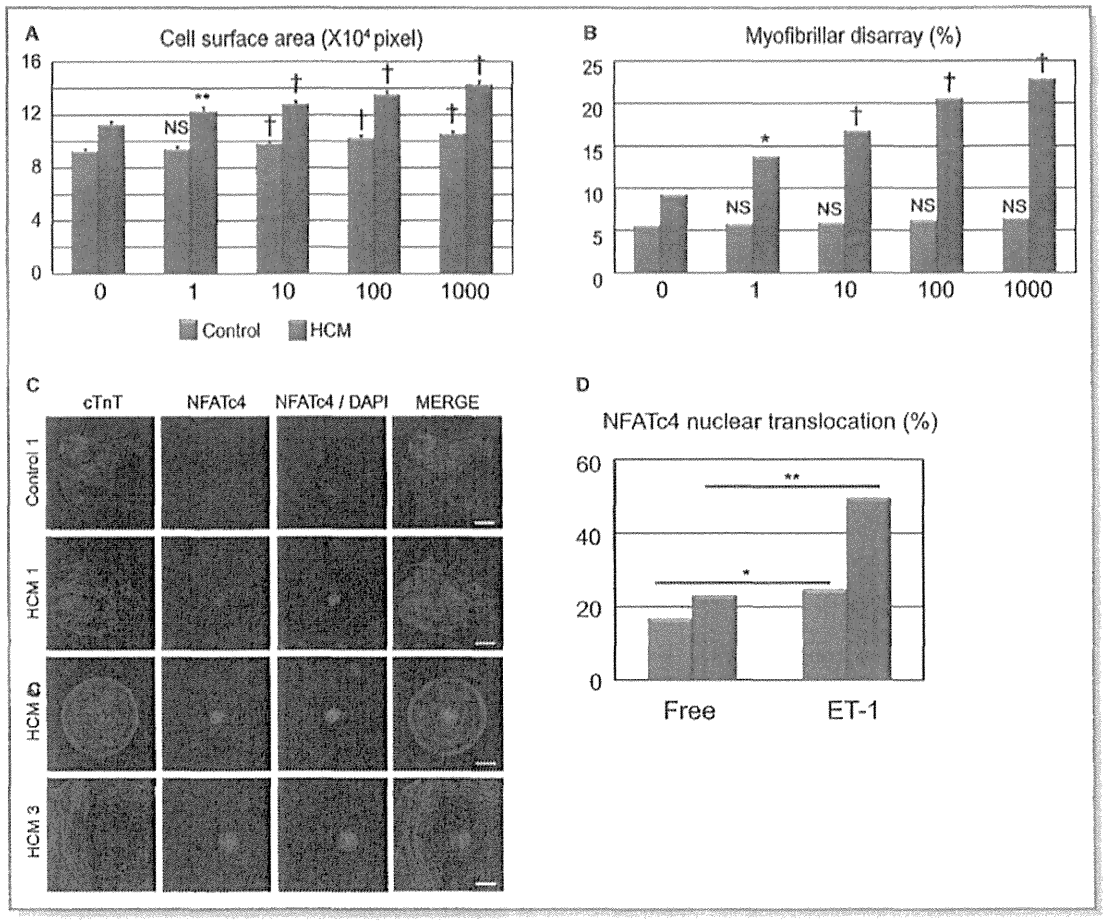

Figure 12. ET-1 strengthens pathological features in HCM iPSC-derived cardiomyocytes in a concentration-dependent manner. A, Cell surface areas of 789 to 822 randomly chosen cardiac troponin-T (cTnT)-positive cardiomyocytes in each group and condition were measured. The cardiomyocytes were dissociated from EBs at 60 days and cultured for 7 days with various concentrations of ET-1 (1, 10, 100, or 1000 nmol/L) (1-way ANOVA with Steel's multiple comparison post-test). B, The percentages of cardiomyocytes with myofibrillar disarray were assessed by immunostaining for cTnT of the single cardiomyocytes after 7 days of culture with ET-1. N=875 to 995 (per each group and condition). *P<0.05, **P<0.01, †P<0.0001 vs ET-1–free (0 nmol/L) condition in the same group (χ^2 test). C and D, Nuclear translocation of NFATc4 was assessed by immunostaining for NFATc4 and cTnT. Isolated cardiomyocytes at 60 days were cultured for 7 days with or without ET-1. The presented images were the iPSC-derived cardiomyocytes cultured for 7 days with ET-1. Scale bars, 20 μm. N=376 to 448 (per each group and condition). *P<0.01, **P<0.001 vs free condition in each group (χ^2 test). EBs indicates0 embryoid bodies; ET-1, endothelin-1; HCM, hypertrophic cardiomyopathy; iPSC, induced pluripotent stem cell; NFAT, nuclear factor of activated T cells.

and HCM iPSC-derived cardiomyocytes showed a single sharp peak with lower SD scores, although the SD scores of HCM were mildly higher than those of control (Figure 17B and Video clip S1). After ET-1 administration, the control iPSC-derived cardiomyocyte histograms still showed a sharp peak at 24 and 48 hours, indicating synergistic beating in a given direction (Figure 17A, 17C, and 17D). In contrast, the HCM iPSC-derived cardiomyocyte histograms showed a broad distribution with higher SD scores after the ET-1 administration, indicating disorganized contractile form (Figure 17A and Video clip S2). The SD scores of the HCM iPSC-derived cardiomyocytes were significantly increased by ET-1 administration at 24 hours compared with the control cells (Figure 17C). At 48 hours, ET-1 administration strongly induced the contractile dispersion in the HCM iPSC-derived cardiomyocytes, and this effect was clearly blocked by ETA-b, but not by ETB-b (Figure 17D).

Discussion

In this study, we elucidated an interaction between genetic backgrounds and environmental factors by using HCM iPSC-

Downloaded from http://jaha.ahajournals.org/ at KEIO UNIVIVERSITY on February 15, 2015

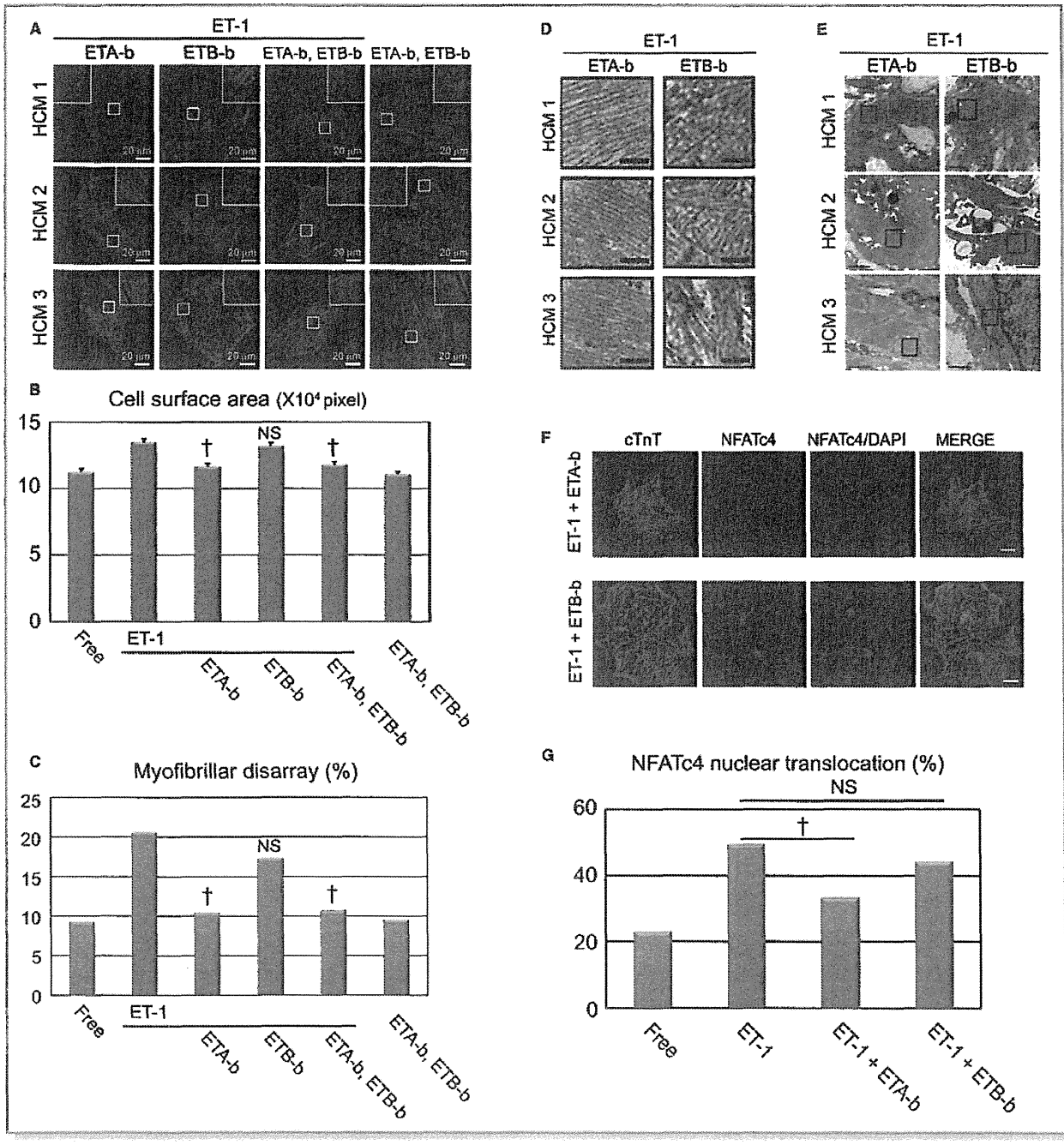

Figure 13. ET-1–ETA axis has a pivotal role in pathological deterioration in HCM iPSC-derived cardiomyocytes. A, Immunostaining for cardiac troponin-T (cTnT) of the single cardiomyocytes derived from HCM 1, HCM 2, and HCM 3 iPSC-derived cardiomyocytes. The single cardiomyocytes at 60 days were cultured for 7 days with ETA-b and/or ETB-b in the presence or absence of ET-1. B, Cell surface areas of 809 to 825 randomly chosen cTnT-positive cardiomyocytes in each condition were measured (1-way ANOVA with Steel's multiple comparison post-test). C, The percentages of cardiomyocytes with myofibrillar disarray were assessed by immunostaining for cTnT of the single cardiomyocytes. N=880 to 995 (per each condition). †P<0.0001 vs ET-1 condition (χ^2 test). D, Electron microscopic observation of beating EBs at 60 days cultured with ETA-b or ETB-b in the presence of ET-1. Scale bars, 200 nm. E, Lower magnified electron microscopic images corresponding with (D). F and G, Nuclear translocation of NFATc4 was assessed by immunostaining for NFATc4 and cTnT. The single cardiomyocytes at 60 days were cultured for 7 days with ETA-b and/or ETB-b in the presence of ET-1. Scale bars, 20 μm. N=391 to 751 (per each culture condition). †P<0.0001 vs ET-1 condition (χ^2 test). EBs indicates embryoid bodies; ET-1, endothelin-1; ETA-b, endothelin receptor type A blocker; ETB-b, endothelin receptor type B blocker; HCM, hypertrophic cardiomyopathy; iPSC, induced pluripotent stem cell; NFAT, nuclear factor of activated T cells.

Downloaded from http://jaha.ahajournals.org/ at KEIO UNIVIVERSITY on February 15, 2015

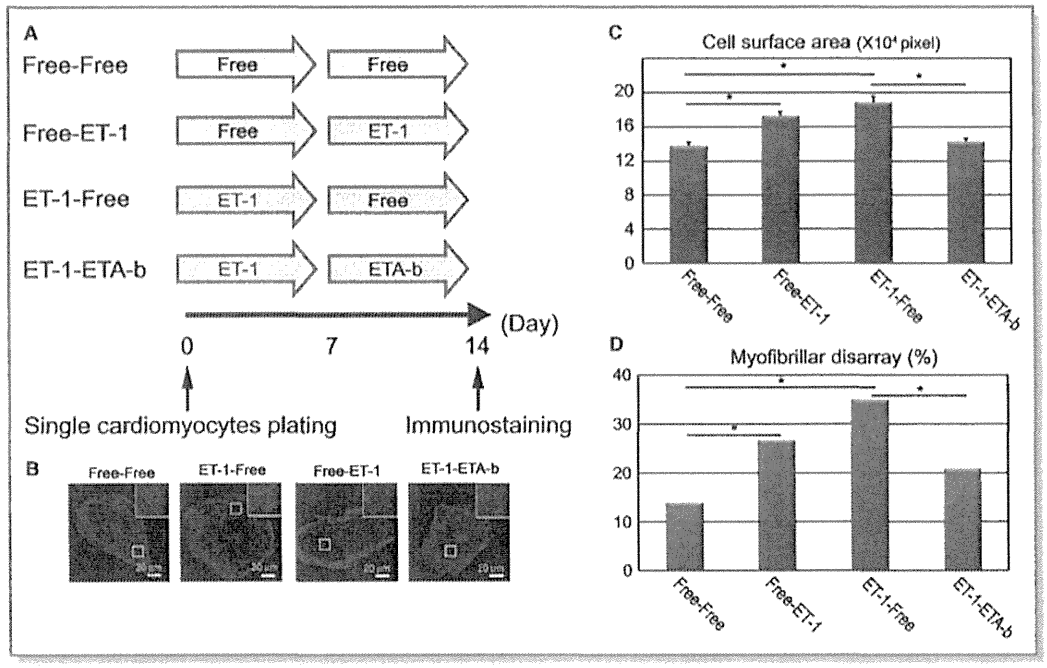

Figure 14. ETA-b regresses the HCM pathological phenotype. A, Time course of drug stimulation protocols for beating single cardiomyocytes. The single cardiomyocytes derived from each of the HCM iPSCs, which were dissociated from EBs at 60 days, were cultured for 7 days with or without ET-1, and then subsequently cultured for 7 days with or without ETA-b. Immunostainings for cTnT with DAPI nuclear staining were performed at 14 days. B, The isolated cardiomyocytes at 60 days were cultured for 7 days with or without ET-1 and subsequently cultured for 7 days with or without ET-1, or ETA-b. C, Cell surface areas of total 300 randomly chosen cTnT-positive cardiomyocytes were measured in each culture condition (1-way ANOVA with Steel's multiple-comparison post-test). D, The percentages of cardiomyocytes with myofibrillar disarray were assessed by immunostaining for cTnT of the single cardiomyocytes. N=317 to 361 (per each culture condition). *P<0.001 (χ^2 test). cTnT indicates cardiac troponin-T; EBs, embryoid bodies; ET-1, endothelin-1; ETA-b, endothelin receptor type A blocker; HCM, hypertrophic cardiomyopathy; iPSCs, induced pluripotent stem cells.

derived cardiomyocytes. HCM patients have a wide variety of medical backgrounds in terms of clinical severity, family history, and gene mutations. However, HCM patients show similar phenotypes in terms of heart morphology, pathology, and hemodynamic features. We therefore sought to identify a common pathway of disease manifestation in HCM among patients with different backgrounds by using iPSC-derived cardiomyocytes. Hence, we selected the patient with HCM without known mutations and the patient with HCM with a mutation in *MYBPC3*, which is one of the most frequent mutated genes in HCM patients.[10]

In HCM hearts, left ventricular hypertrophy and myocardial disarray are key hallmarks as pathological features. These accumulating data definitely suggest that histopathological studies in HCM could provide valuable information in terms of prognosis and disease severity. Myofibrillar disarray is also documented as a HCM phenotype and used as a marker of the disease.[20–22] We found myofibrillar disarray frequently in the HCM iPSC-derived cardiomyocytes. Thereafter, we focused on what could induce this morphological feature and found that the incidence of the myofibrillar disarray was enhanced by ET-1 in the HCM iPSC-derived cardiomyocytes. We also confirmed that cardiomyocytes from established mouse HCM model[16,27] also showed myofibrillar disarray induced by ET-1. In iPSC-derived cardiomyocytes, the expression levels of ET receptors were comparable, but NFAT was activated by ET-1 specifically in the HCM iPSC-derived cardiomyocytes, which suggests that ET-1–induced NFAT activation is intracellularly affected in the HCM iPSC-derived cardiomyocytes. The activation of calcium-dependent serine–threonine protein phosphatase calcineurin induces pathological cardiac hypertrophy and deleterious remodeling of the heart through NFAT activation.[28] On the contrary, the calcineurin–NFAT pathway is not activated in physiological hypertrophic response despite increased systolic calcium transient,[29] the mechanism of which remains unclear.

HCM mutations are found in many sarcomeric genes, including *MYBPC3*. Sarcomere and myofibril formations are finely and tightly regulated. The structural changes could be

Downloaded from http://jaha.ahajournals.org/ at KEIO UNIVIVERSITY on February 15, 2015

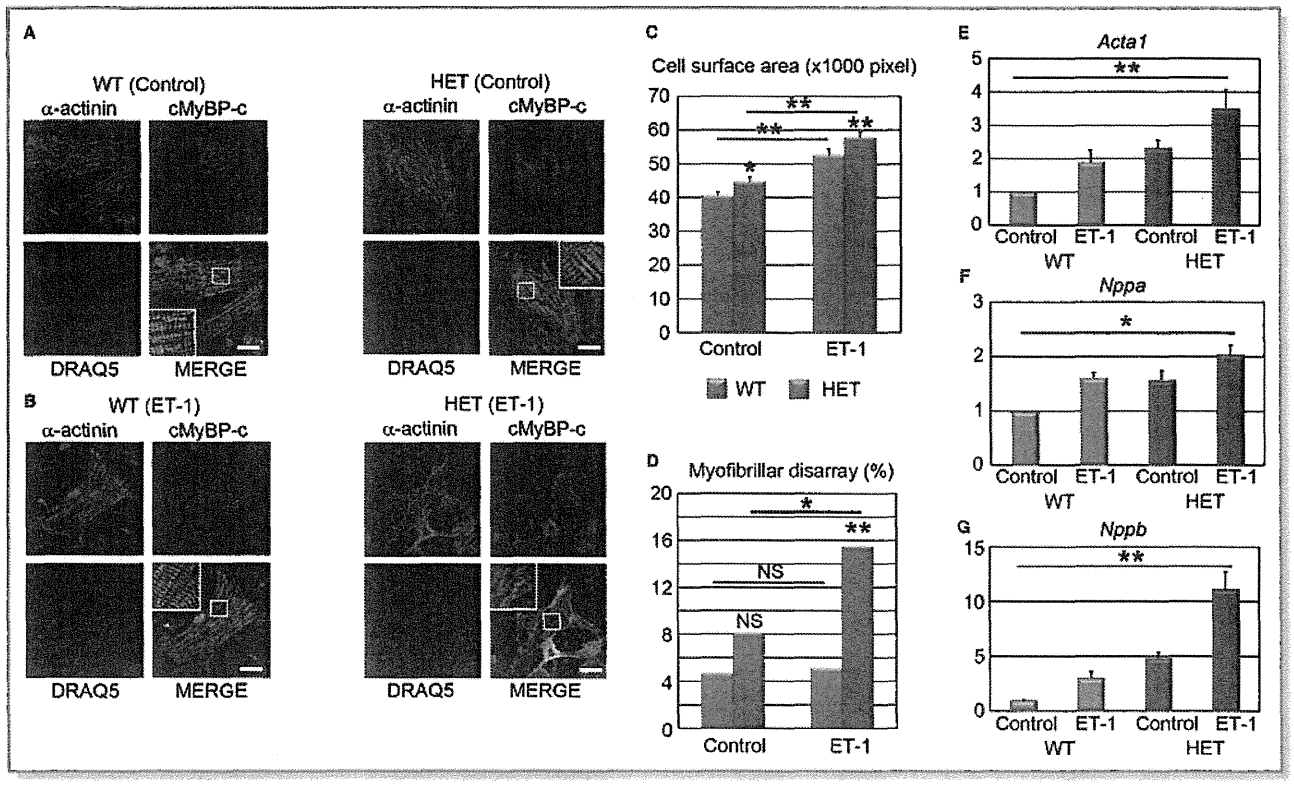

Figure 15. ET-1 augments the incidence of myofibrillar disarray in cardiomyocytes isolated from heterozygous *Mybpc3*-targeted knock-in mice. A, Immunostaining for α-actinin and cMyBP-C with DRAQ5 nuclear staining of cardiomyocytes derived from neonatal wild-type (WT) and *Mybpc3*-targeted heterozygous knock-in (HET) mice. Scale bars, 20 μm. B, Immunostaining for α-actinin and cMyBP-C with DRAQ5 nuclear staining of the single cardiomyocytes derived from WT and HET mice, which were cultured with ET-1 for 48 hours. Scale bars, 20 μm. C, Cell surface areas of 173 to 178 randomly chosen α-actinin–positive cardiomyocytes in each condition were measured. **P*<0.05, ***P*<0.01 vs WT or as indicated on the figure (Mann–Whitney *U* test). D, The percentages of cardiomyocytes with myofibrillar disarray were assessed by immunostaining for α-actinin of the single cardiomyocytes. N=215 to 236. **P*<0.05, ***P*<0.01 vs WT or as indicated on the figure (χ^2 test). E through G, Quantitative RT-PCR analyses for *Acta1*, *Nppa*, and *Nppb*. N=3 to 5. **P*<0.05, ***P*<0.01 (Kruskal–Wallis test). *Acta1* indicates α-skeletal muscle; cMyBP-C, cardiac myosin-binding protein C; ET-1, endothelin-1; *Mybpc3*, human/mouse gene encoding cardiac myosin-binding protein C; *Nppa*, natriuretic peptide type A; *Nppb*, natriuretic peptide type B; RT-PCR, reverse transcription-polymerase chain reaction.

affected by those mutations.[30] The efficiency of incorporation of mutated sarcomeric proteins into sarcomere varies according to the mutation, which could affect the myocyte contractility.[31] The content of mutated protein would vary from fiber to fiber, which would cause variation in force generation in each fiber,[32] which might result in myofibrillar disarray. Several signaling molecules could modify the pathophysiology of HCM in a context-dependent fashion.[3] ET-1, angiotensin, and catecholamines have various important roles, but each ligand has definitely different roles in cardiac physiology.[33] In the heart, binding and activation of ETA predominantly mediate ET-1 signaling and potently induce cardiomyocyte hypertrophy.[34] In our study, ET-1 stimulation specifically induces NFAT nuclear accumulation in the HCM iPSC-derived cardiomyocytes and shows the prominent effects on HCM phenotypes. NFAT is a strong mediator in cardiac hypertrophy and is both sufficient and necessary for the cardiac hypertrophic response.[35,36] Therefore, we have speculated that NFAT activation would exaggerate myofibrillar disarray, which might be slightly present without those stimulation in the presence of sarcomeric gene mutation. To elucidate the physiological effect of myofibrillar disarray, we used high-speed imaging and revealed that the contractile cooperativity was disrupted in the individual HCM iPSC-derived cardiomyocytes. To develop the automated high throughput screening for drug screening, we should determine the suitable markers. Myofibrillar disarray and the contractile cooperativity disruption may be useful markers in HCM cardiomyocytes. Thus, our results will push ahead with the developments of drug invention strategy focused on the underlying pathogenesis of HCM.

This study has several limitations. First, the iPSCs that we used were generated from 2 original cell sources: dermal

Downloaded from http://jaha.ahajournals.org/ at KEIO UNIVIVERSITY on February 15, 2015

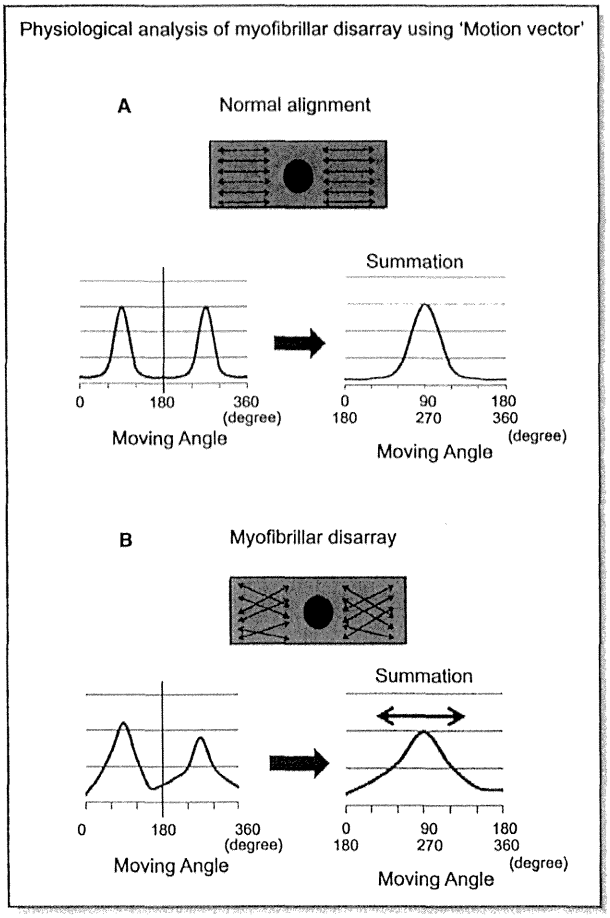

Figure 16. Schema of motion vector analysis for single beating cardiomyocytes. A, Normal cardiomyocytes, beating synchronously in 1 direction, show symmetrical twin peaks under 360° analyses. The summation data indicates a single peak with lower SD scores. B, Cardiomyocytes with myofibrillar disarray, beating nonsynchronously, show ≥2 morphologically irregular peaks under 360° analyses. The summation data indicate flattened peak with higher SD score (double-headed red arrow).

fibroblasts and circulating T lymphocytes. Although the original cell memory would remain in the established iPSCs, it is still unknown if cardiomyocytes differentiated from such iPSCs might inherit the original cell nature. Fibroblasts are often used for the sources of iPSC generation, and the character of iPSC-derived cardiomyocytes was comparable to embryonic stem cell–derived cardiomyocytes.[37] T cell-derived iPSCs could also differentiate into functional cardiomyocytes which are comparable to embryonic stem cell–derived cardiomyocytes,[38] which suggests that those iPSC-derived cardiomyocytes can be used for the disease analysis. Second, the iPSC-derived cardiomyocytes showed immature phenotype, and there should be some differences between adult cardiomyocytes and iPSC-derived cardiomyocytes. Although there are many attempts to obtain mature iPSC-derived cardiomyocytes resembling adult phenotype, ideally rod-shaped cardiomyocytes, current techniques could not accomplish the full maturation. However, we found some pathological differences between control and HCM iPSCs-derived cardiomyocytes, as seen in the previous studies using disease-specific iPSCs. It would be, therefore, an appropriate model to decipher the characteristic differences at the cellular level, though there should be some room for better technical improvement. Third, 3 patients have totally different independent genetic backgrounds. HCM3 has a *MYBPC3* mutation (Gly999-Gln1004del). During further genetic screening, we found that HCM1 has a mutation in *TPM1* (Arg91Cys), but it remains unclear whether the mutation would affect disease phenotype. HCM2 is genetically negative but there may be unknown mutation. It may be possible that those different genetic backgrounds modify disease phenotypic severity. It is preferable to conduct those experiments using many iPSC lines derived from many patients, as with a clinical study. In the future, we would like to recruit many more patients, and detailed characterization will be desired for the patients with independent genetic backgrounds.

HCM mutations induce dysfunction in myocyte contractility, consequently leading to an activation of several stress-responsive trophic and mitotic factors.[39] Because of the lack of human models in which to assess the interactions between genetic backgrounds and such factors, determination of the candidates for HCM progression has been hampered. As used here, emerging iPSC technology enabled us to evaluate this problem, revealing the pathological effects of ET-1. ET-1 is a potent vasoconstrictor that induced hypertrophy in cultured cardiomyocytes,[33] and it is reported that the plasma level of ET-1 was significantly increased in HCM patients.[40,41] The concentration of ET-1 used in the present study was higher than the plasma concentration in patients with heart failure but is the standard ET-1 concentration as used in previous experiments,[42] which would be partly because the ET-1 signal acts in the heart in an autocrine/paracrine fashion.[43] ETA receptor was highly expressed in heart compared with the ETB receptor,[44] and ETA-b attenuated cardiac hypertrophy provoked by several causes.[45,46] In the current study, we showed that the ET-1–ETA axis could be a common pathway in HCM disease manifestation. To move those findings forward to clinical study, we should confirm therapeutic effect of ET-1 blocker on HCM in experimental models in vivo. It is important to know the effect of ET-1 blocker on an in vivo HCM model for various time courses: young age and old age. A transgenic rabbit model of HCM clearly showed temporal evolution of cardiac phenotypes such as a higher calcium sensitivity of myofibrillar ATPase activity at earlier stage and cardiac hypertrophy and fibrosis at later stage, which suggests the

Downloaded from http://jaha.ahajournals.org/ at KEIO UNIVIVERSITY on February 15, 2015

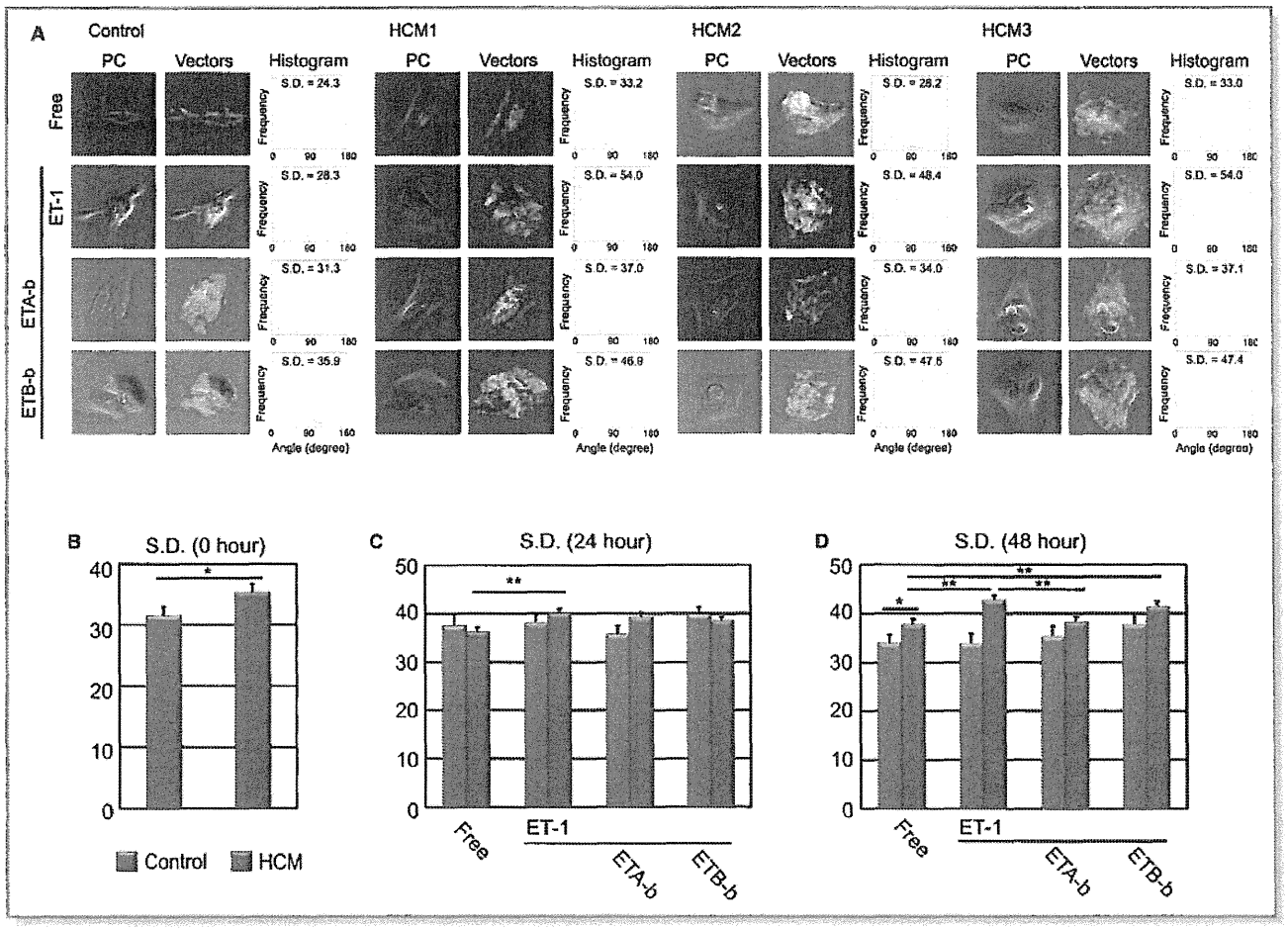

Figure 17. Motion vector analysis of single beating cardiomyocytes derived from control and HCM iPSCs. A, The iPSC-derived single cardiomyocytes at 60 days, which were cultured for 24 hours, were stimulated for 48 hours with or without ET-1 and/or each endothelin receptor blocker. Phase contrast image (PC) showed the single beating cardiomyocytes obtained in this system. Vectors showed traced motion vectors overlaid in the cardiomyocyte image in PC. A histogram showed the frequency of the motion vector angles (angles between each vector and *x*-axis [horizontal axis] in the image) in a single cardiomyocyte. The histograms and SD scores were calculated at 0, 24, and 48 hours after stimulation. B, The SD scores of the vector angle histograms in control and HCM iPSC-derived beating cardiomyocytes before ET-1 stimulation (0 hour). N=30 (control) or 90 (HCM). C, The SD scores of the vector angle histograms after 24-hour stimulation. N=21 to 24 (control) or 79 to 87 (HCM). D, The SD scores of the vector angle histograms after 48-hour stimulation. The SD scores of HCM iPSC-derived cardiomyocytes with ETA-b were significantly reduced, compared with those of ET-1. N=27 to 28 (control) or 67 to 73 (HCM). **P*<0.05, ***P*<0.01 vs as indicated on the figure (Student *t* test). ET-1 indicates endothelin-1; ETA-b, endothelin receptor type A blocker; ETB-b, endothelin receptor type B blocker; HCM, hypertrophic cardiomyopathy; iPSCs, induced pluripotent stem cells.

involvement of multiple independent mechanisms in the pathogenesis of HCM phenotypes.[47]

In summary, we demonstrated that patient-specific iPSCs are invaluable systems in which to assess the genetic–environmental interactions involved in HCM disease progression. Moreover, our data indicate that interactions between the genetic backgrounds and the environmental factor "ET-1" promoted the HCM phenotypes, such as myocyte hypertrophy and myofibrillar disarray, in the HCM iPSC-derived and in the well-characterized HCM mouse model–derived cardiomyocytes. These results could provide useful knowledge regarding the precise disease mechanism that operates downstream of HCM causal mutations to modify the nature of each individual disease state.

Acknowledgments

We thank Dr T. Hayakawa and Mr T. Kunihiro from Sony Corporation for their technical help in the high-speed video recording of cardiomyocytes and in the image analysis with motion vector prediction algorithm. We thank C. Kadota for technical assistance. We thank Thomas Eschenhagen for the thoughtful discussion on experiments we performed in the Department of Experimental Pharmacology and Toxicology, University Medical Center Hamburg-Eppendorf, Hamburg, Germany.

Downloaded from http://jaha.ahajournals.org/ at KEIO UNIVIVERSITY on February 15, 2015

Sources of Funding

This study was supported in part by research grants from the Ministry of Education, Culture, Sports, Science and Technology, Health Labour Sciences Research Grant, the New Energy and Industrial Technology Development Organization, Japan, the Program for Promotion of Fundamental Studies in Health Science of the National Institute of Biomedical Innovation, Japan Science and Technology Agency, Research Center Network for Realization of Regenerative Medicine "The Program for Intractable Diseases Research utilizing Disease-specific iPS cells," The Nakatomi Foundation, Japan Heart Foundation/Novartis Grant for Research Award on Molecular and Cellular Cardiology SENSHIN Medical Research Foundation, Kimura Memorial Heart Foundation Research Grant, Japan Intractable Diseases Research Foundation, Japan, The Cell Science Research Foundation, The Tokyo Biochemical Research Foundation, Suzuken Memorial Foundation, The Japan Foundation for Applied Enzymology, Joint Usage/Research Program of Medical Research Institute, Tokyo Medical and Dental University, the DZHK (German Center for Cardiovascular Research), the German Ministry of Research and Education (BMBF), and the Association Institut de Myologie (Paris).

Disclosures

None.

References

1. Members WC, Gersh BJ, Maron BJ, Bonow RO, Dearani JA, Fifer MA, Link MS, Naidu SS, Nishimura RA, Ommen SR, Rakowski H, Seidman CE, Towbin JA, Udelson JE, Yancy CW. 2011 ACCF/AHA guideline for the diagnosis and treatment of hypertrophic cardiomyopathy: executive summary: a report of the American College of Cardiology Foundation/American Heart Association Task Force on Practice Guidelines. *Circulation*. 2011;124:2761–2796.
2. Coats CJ, Hollman A. Hypertrophic cardiomyopathy: lessons from history. *Heart*. 2008;94:1258–1263.
3. Ashrafian H, McKenna WJ, Watkins H. Disease pathways and novel therapeutic targets in hypertrophic cardiomyopathy. *Circ Res*. 2011;109:86–96.
4. McConnell BK, Fatkin D, Semsarian C, Jones KA, Georgakopoulos D, Maguire CT, Healey MJ, Mudd JO, Moskowitz IPG, Conner DA, Giewat M, Wakimoto H, Berul CI, Schoen FJ, Kass DA, Seidman CE, Seidman JG. Comparison of two murine models of familial hypertrophic cardiomyopathy. *Circ Res*. 2001;88:383–389.
5. Marian AJ. Pathogenesis of diverse clinical and pathological phenotypes in hypertrophic cardiomyopathy. *Lancet*. 2000;355:58–60.
6. Takahashi K, Tanabe K, Ohnuki M, Narita M, Ichisaka T, Tomoda K, Yamanaka S. Induction of pluripotent stem cells from adult human fibroblasts by defined factors. *Cell*. 2007;131:861–872.
7. Khan JM, Lyon AR, Harding SE. The case for induced pluripotent stem cell-derived cardiomyocytes in pharmacological screening. *Br J Pharmacol*. 2013;169:304–317.
8. Tiscornia G, Vivas EL, Belmonte JCI. Diseases in a dish: modeling human genetic disorders using induced pluripotent cells. *Nat Med*. 2011;17:1570–1576.
9. Force T, Bonow RO, Houser SR, Solaro RJ, Hershberger RE, Adhikari B, Anderson ME, Boineau R, Byrne BJ, Cappola TP, Kalluri R, LeWinter MM, Maron MS, Molkentin JD, Ommen SR, Regnier M, Tang WHW, Tian R, Konstam MA, Maron BJ, Seidman CE. Research priorities in hypertrophic cardiomyopathy. *Circulation*. 2010;122:1130–1133.
10. Behrens-Gawlik V, Mearini G, Gedicke-Hornung C, Richard P, Carrier L. MYBPC3 in hypertrophic cardiomyopathy: from mutation identification to RNA-based correction. *Pflugers Arch*. 2014;466:215–223.
11. Marian AJ. Experimental therapies in hypertrophic cardiomyopathy. *J Cardiovasc Transl Res*. 2009;2:483–492.
12. Hayakawa T, Kunihiro T, Dowaki S, Uno H, Matsui E, Uchida M, Kobayashi S, Yasuda A, Shimizu T, Okano T. Noninvasive evaluation of contractile behavior of cardiomyocyte monolayers based on motion vector analysis. *Tissue Eng Part C Methods*. 2012;18:21–32.
13. Ohnuki M, Takahashi K, Yamanaka S. Generation and characterization of human induced pluripotent stem cells. *Curr Protoc Stem Cell Biol*. John Wiley & Sons, Inc; 2009;9:4A.2. 1–25.
14. Seki T, Yuasa S, Fukuda K. Generation of induced pluripotent stem cells from a small amount of human peripheral blood using a combination of activated T cells and Sendai virus. *Nat Protoc*. 2012;7:718–728.
15. Seki T, Yuasa S, Fukuda K. Derivation of induced pluripotent stem cells from human peripheral circulating T cells. *Curr Protoc Stem Cell Biol*. John Wiley & Sons, Inc; 2011;18:4A.3. 1–9.
16. Vignier N, Schlossarek S, Fraysse B, Mearini G, Krämer E, Pointu H, Mougenot N, Guiard J, Reimer R, Hohenberg H, Schwartz K, Vernet M, Eschenhagen T, Carrier L. Nonsense-mediated mRNA decay and ubiquitin–proteasome system regulate cardiac myosin-binding protein C mutant levels in cardiomyopathic mice. *Circ Res*. 2009;105:239–248.
17. Seki T, Yuasa S, Oda M, Egashira T, Yae K, Kusumoto D, Nakata H, Tohyama S, Hashimoto H, Kodaira M, Okada Y, Seimiya H, Fusaki N, Hasegawa M, Fukuda K. Generation of induced pluripotent stem cells from human terminally differentiated circulating T cells. *Cell Stem Cell*. 2010;7:11–14.
18. Egashira T, Yuasa S, Suzuki T, Aizawa Y, Yamakawa H, Matsuhashi T, Ohno Y, Tohyama S, Okata S, Seki T, Kuroda Y, Yae K, Hashimoto H, Tanaka T, Hattori F, Sato T, Miyoshi S, Takatsuki S, Murata M, Kurokawa J, Furukawa T, Makita N, Aiba T, Shimizu W, Horie M, Kamiya K, Kodama I, Ogawa S, Fukuda K. Disease characterization using LQTS-specific induced pluripotent stem cells. *Cardiovasc Res*. 2012;95:419–429.
19. Maron BJ, Gottdiener JS, Epstein SE. Patterns and significance of distribution of left ventricular hypertrophy in hypertrophic cardiomyopathy. *Am J Cardiol*. 1981;48:418–428.
20. Tashiro A, Masuda T, Segawa I. Morphometric comparison of mitochondria and myofibrils of cardiomyocytes between hypertrophic and dilated cardiomyopathies. *Virchows Arch A Pathol Anat Histopathol*. 1990;416:473–478.
21. Pearce PC, Hawkey C, Symons C, Olsen EG. Role of calcium in the induction of cardiac hypertrophy and myofibrillar disarray. Experimental studies of a possible cause of hypertrophic cardiomyopathy. *Br Heart J*. 1985;54:420–427.
22. Kim SJ, Iizuka K, Kelly RA, Geng YJ, Bishop SP, Yang G, Kudej A, McConnell BK, Seidman CE, Seidman JG, Vatner SF. An alpha-cardiac myosin heavy chain gene mutation impairs contraction and relaxation function of cardiac myocytes. *Am J Physiol*. 1999;276:H1780–H1787.
23. van Dijk SJ, Dooijes D, dos Remedios C, Michels M, Lamers JMJ, Winegrad S, Schlossarek S, Carrier L, ten Cate FJ, Stienen GJM, van der Velden J. Cardiac myosin-binding protein C mutations and hypertrophic cardiomyopathy: haploinsufficiency, deranged phosphorylation, and cardiomyocyte dysfunction. *Circulation*. 2009;119:1473–1483.
24. Marston S, Copeland ON, Gehmlich K, Schlossarek S, Carrrier L. How do MYBPC3 mutations cause hypertrophic cardiomyopathy? *J Muscle Res Cell Motil*. 2012;33:75–80.
25. Poirier O, Nicaud V, McDonagh T, Dargie HJ, Desnos M, Dorent R, Roizes G, Schwartz K, Tiret L, Komajda M, Cambien F. Polymorphisms of genes of the cardiac calcineurin pathway and cardiac hypertrophy. *Eur J Hum Genet*. 2003;11:659–664.
26. Jandeleit-Dahm KAM, Watson AMD. The endothelin system and endothelin receptor antagonists. *Curr Opin Nephrol Hypertens*. 2012;21:66–71.
27. Fraysse B, Weinberger F, Bardswell SC, Cuello F, Vignier N, Geertz B, Starbatty J, Krämer E, Coirault C, Eschenhagen T, Kentish JC, Avkiran M, Carrier L. Increased myofilament Ca^{2+} sensitivity and diastolic dysfunction as early consequences of Mybpc3 mutation in heterozygous knock-in mice. *J Mol Cell Cardiol*. 2012;52:1299–1307.
28. Molkentin JD. Parsing good versus bad signaling pathways in the heart: role of calcineurin–nuclear factor of activated T-cells. *Circ Res*. 2013;113:16–19.
29. Wilkins BJ, Dai Y-S, Bueno OF, Parsons SA, Xu J, Plank DM, Jones F, Kimball TR, Molkentin JD. Calcineurin/NFAT coupling participates in pathological, but not physiological, cardiac hypertrophy. *Circ Res*. 2004;94:110–118.
30. Marian AJ, Roberts R. The molecular genetic basis for hypertrophic cardiomyopathy. *J Mol Cell Cardiol*. 2001;33:655–670.

Downloaded from http://jaha.ahajournals.org/ at KEIO UNIVIVERSITY on February 15, 2015

31. Yang Q, Sanbe A, Osinska H, Hewett TE, Klevitsky R, Robbins J. A mouse model of myosin binding protein C human familial hypertrophic cardiomyopathy. *J Clin Invest*. 1998;102:1292–1300.
32. Kirschner SE, Becker E, Antognozzi M, Kubis H-P, Francino A, Navarro-López F, Bit-Avragim N, Perrot A, Mirrakhimov MM, Osterziel K-J, McKenna WJ, Brenner B, Kraft T. Hypertrophic cardiomyopathy-related β-myosin mutations cause highly variable calcium sensitivity with functional imbalances among individual muscle cells. *Am J Physiol*. 2005;288:H1242–H1251.
33. Kang M, Chung KY, Walker JW. G-protein coupled receptor signaling in myocardium: not for the faint of heart. *Physiology*. 2007;22:174–184.
34. Sugden PH. An overview of endothelin signaling in the cardiac myocyte. *J Mol Cell Cardiol*. 2003;35:871–886.
35. Molkentin JD, Lu J-R, Antos CL, Markham B, Richardson J, Robbins J, Grant SR, Olson EN. A calcineurin-dependent transcriptional pathway for cardiac hypertrophy. *Cell*. 1998;93:215–228.
36. Wilkins BJ, Molkentin JD. Calcineurin and cardiac hypertrophy: where have we been? Where are we going? *J Physiol*. 2002;541:1–8.
37. Zhang J, Wilson GF, Soerens AG, Koonce CH, Yu J, Palecek SP, Thomson JA, Kamp TJ. Functional cardiomyocytes derived from human induced pluripotent stem cells. *Circ Res*. 2009;104:e30–e41.
38. Seki T, Yuasa S, Kusumoto D, Kunitomi A, Saito Y, Tohyama S, Yae K, Kishino Y, Okada M, Hashimoto H, Takei M, Egashira T, Kodaira M, Kuroda Y, Tanaka A, Okata S, Suzuki T, Murata M, Fujita J, Fukuda K. Generation and characterization of functional cardiomyocytes derived from human T cell-derived induced pluripotent stem cells. *PLoS One*. 2014;9:e85645.
39. Östman-Smith I, Wettrell G. Pathophysiology of hypertrophic cardiomyopathy. *Lancet*. 2000;355:928.
40. Ito H, Hirata Y, Hiroe M, Tsujino M, Adachi S, Takamoto T, Nitta M, Taniguchi K, Marumo F. Endothelin-1 induces hypertrophy with enhanced expression of muscle-specific genes in cultured neonatal rat cardiomyocytes. *Circ Res*. 1991;69:209–215.
41. Hasegawa K, Fujiwara H, Koshiji M, Inada T, Ohtani S, Doyama K, Tanaka M, Matsumori A, Fujiwara T, Shirakami G, Hosoda K, Nakao K, Sasayama S. Endothelin-1 and its receptor in hypertrophic cardiomyopathy. *Hypertension*. 1996;27:259–264.
42. Kedzierski RM, Yanagisawa M. Endothelin system: the double-edged sword in health and disease. *Annu Rev Pharmacol Toxicol*. 2001;41:851–876.
43. Higazi DR, Fearnley CJ, Drawnel FM, Talasila A, Corps EM, Ritter O, McDonald F, Mikoshiba K, Bootman MD, Roderick HL. Endothelin-1-stimulated InsP3-induced Ca^{2+} release is a nexus for hypertrophic signaling in cardiac myocytes. *Mol Cell*. 2009;33:472–482.
44. Thibault G, Arguin C, Garcia R. Cardiac endothelin-1 content and receptor subtype in spontaneously hypertensive rats. *J Mol Cell Cardiol*. 1995;27:2327–2336.
45. Ito H, Hiroe M, Hirata Y, Fujisaki H, Adachi S, Akimoto H, Ohta Y, Marumo F. Endothelin eta receptor antagonist blocks cardiac hypertrophy provoked by hemodynamic overload. *Circulation*. 1994;89:2198–2203.
46. Ehmke H, Faulhaber J, Münter K, Kirchengast M, Wiesner RJ. Chronic ETA receptor blockade attenuates cardiac hypertrophy independently of blood pressure effects in renovascular hypertensive rats. *Hypertension*. 1999;33:954–960.
47. Nagueh SF, Chen S, Patel R, Tsybouleva N, Lutucuta S, Kopelen HA, Zoghbi WA, Quiñones MA, Roberts R, Marian AJ. Evolution of expression of cardiac phenotypes over a 4-year period in the β-myosin heavy chain-Q403 transgenic rabbit model of human hypertrophic cardiomyopathy. *J Mol Cell Cardiol*. 2004;36:663–673.

Downloaded from http://jaha.ahajournals.org/ at KEIO UNIVIVERSITY on February 15, 2015

Journal of the American Heart Association
OPEN ACCESS
American Heart Association | American Stroke Association

Endothelin–1 Induces Myofibrillar Disarray and Contractile Vector Variability in Hypertrophic Cardiomyopathy–Induced Pluripotent Stem Cell–Derived Cardiomyocytes

Atsushi Tanaka, Shinsuke Yuasa, Giulia Mearini, Toru Egashira, Tomohisa Seki, Masaki Kodaira, Dai Kusumoto, Yusuke Kuroda, Shinichiro Okata, Tomoyuki Suzuki, Taku Inohara, Takuro Arimura, Shinji Makino, Kensuke Kimura, Akinori Kimura, Tetsushi Furukawa, Lucie Carrier, Koichi Node and Keiichi Fukuda

J Am Heart Assoc. 2014;3:e001263; originally published November 11, 2014;
doi: 10.1161/JAHA.114.001263
The *Journal of the American Heart Association* is published by the American Heart Association, 7272 Greenville Avenue, Dallas, TX 75231
Online ISSN: 2047-9980

The online version of this article, along with updated information and services, is located on the World Wide Web at:
http://jaha.ahajournals.org/content/3/6/e001263

Data Supplement (unedited) at:
http://jaha.ahajournals.org/content/suppl/2014/11/11/jah3730.DC1.html

Subscriptions, Permissions, and Reprints: The *Journal of the American Heart Association* is an online only Open Access publication. Visit the Journal at http://jaha.ahajournals.org for more information.

Downloaded from http://jaha.ahajournals.org/ at KEIO UNIVIVERSITY on February 15, 2015

Leukemia (2014) 28, 2344–2354
© 2014 Macmillan Publishers Limited All rights reserved 0887-6924/14
www.nature.com/leu

ORIGINAL ARTICLE

Impaired hematopoietic differentiation of *RUNX1*-mutated induced pluripotent stem cells derived from FPD/AML patients

M Sakurai[1], H Kunimoto[1], N Watanabe[2], Y Fukuchi[1], S Yuasa[3], S Yamazaki[4], T Nishimura[5], K Sadahira[1], K Fukuda[3], H Okano[6], H Nakauchi[4,5], Y Morita[7], I Matsumura[7], K Kudo[8], E Ito[8], Y Ebihara[9], K Tsuji[9,10], Y Harada[11,12], H Harada[11,12], S Okamoto[1] and H Nakajima[1]

Somatic mutation of *RUNX1* is implicated in various hematological malignancies, including myelodysplastic syndrome and acute myeloid leukemia (AML), and previous studies using mouse models disclosed its critical roles in hematopoiesis. However, the role of *RUNX1* in human hematopoiesis has never been tested in experimental settings. Familial platelet disorder (FPD)/AML is an autosomal dominant disorder caused by germline mutation of *RUNX1*, marked by thrombocytopenia and propensity to acute leukemia. To investigate the physiological function of *RUNX1* in human hematopoiesis and pathophysiology of FPD/AML, we derived induced pluripotent stem cells (iPSCs) from three distinct FPD/AML pedigrees (FPD-iPSCs) and examined their defects in hematopoietic differentiation. By *in vitro* differentiation assays, FPD-iPSCs were clearly defective in the emergence of hematopoietic progenitors and differentiation of megakaryocytes, and overexpression of wild-type (WT)-*RUNX1* reversed most of these phenotypes. We further demonstrated that overexpression of mutant-*RUNX1* in WT-iPSCs did not recapitulate the phenotype of FPD-iPSCs, showing that the mutations were of loss-of-function type. Taken together, this study demonstrated that haploinsufficient *RUNX1* allele imposed cell-intrinsic defects on hematopoietic differentiation in human experimental settings and revealed differential impacts of *RUNX1* dosage on human and murine megakaryopoiesis. FPD-iPSCs will be a useful tool to investigate mutant *RUNX1*-mediated molecular processes in hematopoiesis and leukemogenesis.

Leukemia (2014) **28,** 2344–2354; doi:10.1038/leu.2014.136

INTRODUCTION

RUNX1 is a founding member of Runt-family transcription factors, which was cloned from a break point of t(8;21) chromosomal translocation observed in acute myeloid leukemia (AML). Studies over a decade have revealed critical roles of *RUNX1* in hematopoiesis. During embryonic development, *Runx1* is absolutely essential in the emergence of hematopoietic stem and progenitor cells through hemogenic endothelium. In contrast, conditional disruption of *Runx1* in adult hematopoietic system revealed that it was critical in the differentiation of megakaryocytes (MgKs) and lymphocytes as well as in the homeostasis of hematopoietic stem cells.[1] However, these results were mostly derived from gene-disruption studies in mice, and the role of *RUNX1* in human hematopoiesis has never been tested in experimental settings.

Somatic mutation of *RUNX1* has been implicated in a variety of hematological malignancies, including myelodysplastic syndrome (MDS) and AML. It was found in 15–35% cases of AML M0 subtype,[2] 10–20% of MDS,[3–6] 37% of chronic myelomonocytic leukemia[7] and 14% of MDS/myeloproliferative neoplasm,[8] which makes *RUNX1* as one of the most frequently mutated genes in hematological malignancies.

The mutations are distributed throughout *RUNX1* protein, being roughly classified into two categories, missense mutation in N-terminal Runt-homology domain and frame-shift or non-sense mutations leading to a C-terminal truncation. Runt-homology domain mutation impairs DNA-binding and nuclear localization, while the C-terminal truncation disrupts transcriptional activation or repression activity.[3,9] Biochemical studies have shown that most of the *RUNX1* mutations observed in MDS or AML are loss-of-function mutation or dominant negative to the residual wild-type (WT) allele.[9–12] However, their capacities to suppress transcriptional activity of WT-*RUNX1* vary among mutants by *in vitro* assays.[3] In addition, it is possible that some mutations confer the protein with non-physiological functions acting as gain-of-function mutants. Therefore, precise function of mutant *RUNX1* in MDS or AML remains obscure, and it must be tested in physiological and, ideally, in human settings.

Familial platelet disorder/AML(FPD/AML) is a rare autosomal dominant disorder caused by germline mutation of *RUNX1*, marked by thrombocytopenia and propensity to acute leukemia.[13] Approximately 30 FPD/AML pedigrees have been reported to date, and the affected patients retained *RUNX1* mutation at similar positions as reported in MDS and AML. Most patients present no

[1]Division of Hematology, Department of Internal Medicine, Keio University School of Medicine, Tokyo, Japan; [2]Department of Transfusion Medicine and Cell Therapy, Keio University School of Medicine, Tokyo, Japan; [3]Division of Cardiology, Department of Internal Medicine, Keio University School of Medicine, Tokyo, Japan; [4]Japan Science and Technology Agency, ERATO, Tokyo, Japan; [5]Division of Stem Cell Therapy, Center for Stem Cell Biology and Regenerative Medicine, The Institute of Medical Science, The University of Tokyo, Tokyo, Japan; [6]Department of Physiology, Keio University School of Medicine, Tokyo, Japan; [7]Division of Hematology and Rheumatology, Department of Internal Medicine, Kinki University Faculty of Medicine, Osaka, Japan; [8]Department of Pediatrics, Hirosaki University Graduate School of Medicine, Aomori, Japan; [9]Department of Pediatric Hematology/Oncology, The Institute of Medical Science, The University of Tokyo, Tokyo, Japan; [10]Division of Stem Cell Processing, Center for Stem Cell Biology and Regenerative Medicine, The Institute of Medical Science, The University of Tokyo, Tokyo, Japan and [11]Department of Hematology and Oncology, Division of Clinical Research, Research Institute for Radiation Biology and Medicine, Hiroshima University, Hiroshima, Japan. Correspondence: Professor H Nakajima, Division of Hematology, Department of Internal Medicine, Keio University School of Medicine, 35 Shinanomachi, Shinjuku-ku, Tokyo 160-8582, Japan.
E-mail: hnakajim@z2.keio.jp
[12]Present address: Department of Hematology, Juntendo University School of Medicine, Tokyo, Japan.
Received 30 October 2013; revised 30 March 2014; accepted 9 April 2014; accepted article preview online 15 April 2014; advance online publication, 13 May 2014

evident clinical symptoms or developmental abnormalities except mild thrombocytopenia from their childhood. However, approximately half of FPD/AML patients develop MDS or acute leukemia after a long latency, generally after the third decade of their lives. These facts together with insights from mouse studies[14] clearly indicate that *RUNX1* mutation *per se* is not sufficient for leukemia development, but it establishes preleukemic state that predisposes cells to full-blown leukemia by acquiring additional genetic events.[15,16] It is therefore expected that studying the pathogenesis of FPD/AML would provide a valuable insight into the molecular mechanism of leukemia or MDS with *RUNX1* mutation. However, rarity of FPD/AML pedigrees and limited opportunity to obtain their patient samples has tremendously hampered the study.

Induced pluripotent stem cells (iPSCs) provide us with novel opportunities for disease modeling and drug discovery[17,18] Hematopoietic differentiation of iPSCs can be induced by co-culture on stromal cells, and iPSC-derived hematopoietic progenitors can be used further for recapitulating disease phenotypes.[19–27] As iPSCs can be an indefinite source for differentiated cells, they are particularly useful when disease samples cannot be easily obtained from patients.

To investigate the physiological function of *RUNX1* in human hematopoiesis and the pathophysiology of FPD/AML, we derived iPSCs from three distinct FPD/AML pedigrees (FPD-iPSCs) and examined their defects in the emergence of hematopoietic progenitor cells (HPCs) and hematopoietic differentiation. These pedigrees have distinct heterozygous mutations in *RUNX1* gene, two in the N-terminal RUNT domain affecting its DNA-binding activity and one in the C-terminal region affecting its transactivation capacity. Three FPD-iPSC lines uniformly presented a variety of defects in the emergence in HPCs and MgK differentiation, which were rescued by overexpression of WT-*RUNX1*. We further demonstrated that overexpression of mutant-*RUNX1* in WT-iPSCs did not recapitulate the phenotype of FPD-iPSCs, showing that the mutations were of loss-of-function type. Taken together, this study, for the first time, demonstrated that haploinsufficient *RUNX1* allele imposed cell-intrinsic defects on the emergence of HPCs and MgK differentiation in human experimental settings and revealed differential impacts of *RUNX1* dosage on human and murine megakaryopoiesis.

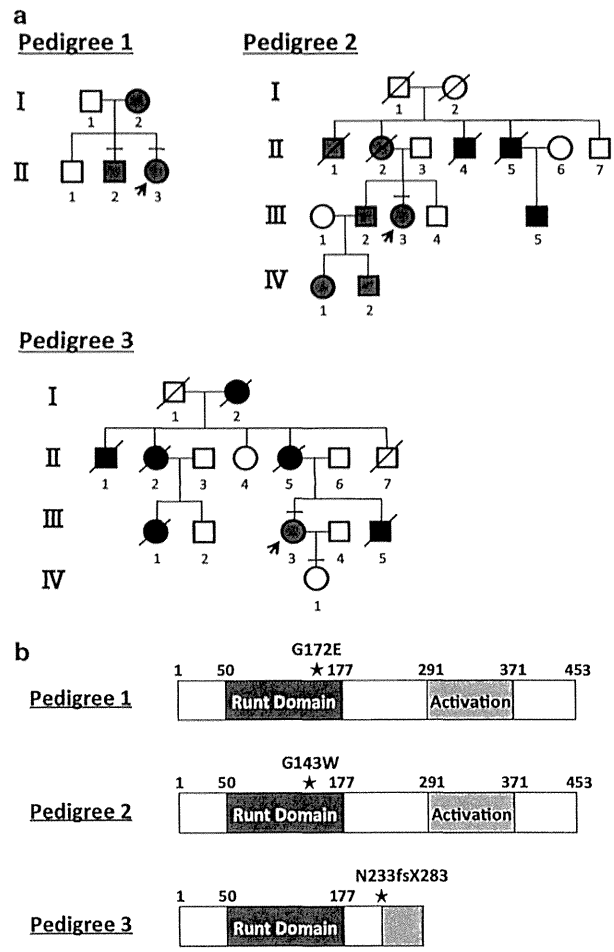

Figure 1. Pedigrees of FPD/AML and sequence analysis of *RUNX1* gene. (**a**) Family trees of three FPD/AML pedigrees. Open symbols, unaffected individuals; gray symbols, patients with thrombocytopenia; black symbols, patients who developed acute leukemia or MDS. Slash lines represent deceased individuals. Arrows denote patients enrolled in the study. (**b**) Summary of *RUNX1* mutations identified in FPD/AML pedigrees. Amino acid numbers are shown on the top of each panel. Positions of mutated amino acids are shown in filled stars. An area with oblique lines denotes irrelevant amino-acid sequence added due to a frame-shift mutation. Activation; transactivation domain.

MATERIALS AND METHODS

Patients

Family trees of three FPD/AML pedigrees are depicted in Figure 1a. Peripheral blood samples from affected patients were collected after obtaining written informed consent. The study was conducted with approval from the internal review board of Keio University School of Medicine, Tokyo, Japan and conformed to the principles outlined in the Declaration of Helsinki for use of human tissue or subjects.

DNA sequence

Genomic DNA was purified by phenol–chloroform method or by QIAamp DNA Micro Kit (Qiagen, Tokyo, Japan) according to the manufacturer's protocol. RUNX1 mutations of iPSCs were verified by direct sequencing of PCR product of *RUNX1* gene amplified from genomic DNA of iPSCs. PCR was performed by PicoMaxx high-fidelity PCR system (Agilent Technologies, Santa Clara, CA, USA) with primers for *RUNX1* that were previously described.[3] PCR products were purified and subjected to direct sequencing by using BigDye Terminator v1.1 Cycle sequencing kit (Life Technologies Japan, Tokyo, Japan) and ABI Prism 310 Genetic Analyzer (Life Technologies Japan).

Generation of iPSCs and cell culture

iPSCs were established from peripheral T cells obtained from patients. Detailed protocol for generating iPSCs from human peripheral blood mononuclear cells was previously described.[28] Control iPSCs were generated from peripheral T cells of healthy male donors after informed consent. Established iPSCs were maintained on inactivated mouse embryonic fibroblasts in iPSC medium, and cells were passaged by treating cells with 1 mg/ml collagenase IV (Life Technologies Japan) every 5–6 days.

Reverse transcription-PCR (RT-PCR)

Total RNA was isolated using TRIZOL reagent (Life Technologies Japan) according to the manufacturer's instructions. cDNA was reverse-transcribed using SuperScript II reverse transcriptase (Life Technologies Japan). PCR was performed using PicoMaxx high-fidelity PCR system (Agilent Technologies) as previously described.[29] Quantitative RT-PCR (qRT-PCR) was performed as previously described.[29] Primer sequences are listed in Supplementary Table S1.

Teratoma formation assay

iPSCs (1×10^7) were injected into the testis of NOD-SCID mice (CLEA Japan, Tokyo, Japan) under anesthesia with pentobarbital sodium (Kyoritsu Seiyaku Corporation, Tokyo, Japan). Eleven weeks after injection, tumors were dissected and fixed in 4% paraformaldehyde in phosphate-buffered-

© 2014 Macmillan Publishers Limited

saline. Fixed tissues were then embedded in paraffin, sectioned and stained with hematoxylin and eosin for analysis.

Immunofluorescence staining

Immunofluorescence staining was performed using the following primary antibodies: anti-NANOG (Abcam, Cambridge, MA, USA), anti-OCT3/4 (Santa Cruz Biotechnology, Dallas, TX, USA), anti-SSEA 3 (Millipore, Billerica, MA, USA), anti-SSEA 4 (Millipore), anti-Tra1-60 (Millipore), and anti-Tra1-81 (Millipore). The secondary antibodies used were: anti-mouse immunoglobulin G (IgG), anti-mouse IgM, anti-rabbit IgG, and anti-rat IgM monoclonal antibodies conjugated with Alexa Fluor 488 or 594 (Life Technologies Japan). Fluorescent images were captured using fluorescence microscope (IX70, Olympus, Tokyo, Japan) with CCD camera (DP70, Olympus).

Hematopoietic differentiation of iPSCs

We used AGM-S3 co-culture [3031] or embryonic stem (ES) sac protocols[32] to assess hematopoietic differentiation of iPSCs as previously described. For AGM-S3 co-culture, iPSCs were plated onto inactivated AGM-S3 cells and cultured for 2–3 days with iPSC medium. On day 2 or 3, medium was replaced with Iscove's modified Dulbecco's medium (Sigma, St Louis, MO, USA) supplemented with 10% fetal bovine serum (Sigma), 20 ng/ml human vascular endothelial growth factor (PeproTech, Rocky Hill, NJ, USA), 1% nonessential amino acid solution (Life Technologies Japan), 100 μM 2-ME (Wako, Osaka, Japan) and 1 mM L-glutamine (Wako). Hematopoietic cells recognized as 'cobble-stone' area surrounding iPS colonies emerge on day 10–14 of co-culture, which are then harvested using 0.05% trypsin/EDTA (Wako) for further experiments.

For ES sac formation, small iPS colonies were transferred onto irradiated C3H10T1/2 cells and co-cultured in Iscove's modified Dulbecco's mediu supplemented with 15% fetal bovine serum, 10 μg/ml human insulin, 5.5 μg/ml human transferrin, 5 ng/ml sodium selenite (Sigma), 2 mM L-glutamine (Life Technologies Japan), 0.45 mM α-monothioglycerol (Sigma), 50 μg/ml ascorbic acid (Sigma) and 20 ng/ml human vascular endothelial growth factor. On days 14 – 15 of culture, sac-like structure containing hematopoietic cells (iPS-sac) formed on the feeders were manually collected into 50-ml tubes, gently crushed with pipetting and passed through a 40-μm cell strainer to obtain hematopoietic progenitors.

Colony-forming assay

$CD34^+$ cells derived from iPSCs by AGM-S3 co-culture were sorted by flow cytometry and subjected to colony-forming assays using Methocult H4435 (Stem Cell Technologies, Vancouver, BC, Canada). Numbers and types of colonies were assessed on day 14.

Flow cytometry

Cells were stained in phosphate-buffered-saline/5% fetal bovine serum with the following monoclonal antibodies: anti-CD34-fluorescein isothiocyanate (FITC), anti-CD45-phycoerythrin (PE), anti-CD31-PE, anti-CD41a-PE, anti-CD42b-FITC (BD Pharmingen, San Jose, CA, USA), anti-glycophorin A (GPA)-FITC and anti-CD43- allophycocyanin (BioLegend, San Diego, CA, USA). Stained cells were analyzed by fluorescence-activated cell sorting (FACS) Calibur with the CellQuest software (BD Biosciences, San Jose, CA, USA) or sorted by MoFlo (Beckman Coulter, Brea, CA, USA). The data were analyzed by the FlowJo software (Tomy Digital Biology, Tokyo, Japan).

Differentiation of MgKs from $CD34^+$ cells

$CD34^+$ cells generated from iPSCs were sorted by flow cytometry and cultured in minimum essential medium alpha (Life Technologies Japan) supplemented with 10% bovine serum albumin, 100 μM 2-ME, 100 ng/ml stem cell factor (PeproTech) and 10 ng/ml thrombopoietin (PeproTech) at 37 °C under hypoxia condition (5% O_2). After 3 days of culture, cells were counted, harvested and analyzed by flow cytometry.

Stable transfection of iPSCs

pcDNA3.1/Flag-WT-*RUNX1* expressing human WT-*RUNX1b* isoform, pcDNA3.1/Flag-*RUNX1*^{G172E} or pcDNA3.1/*RUNX1*^{N233fsX283} was transfected into iPSCs using FuGENE HD transfection reagent (Promega, Madison, WI, USA) according to the manufacturer's protocol. After 2 days of transfection, stable transformants were selected in human ES medium supplemented with 100 μg/ml of G418 (Roche, Basel, Switzerland). Surviving colonies were picked up around day 14 of selection and subjected to further analyses of mRNA and protein expression.

Western blotting

Preparation of protein extracts and western blotting were performed as previously described.[33] Briefly, iPSCs were lysed in the lysis buffer (1% Nonidet P-40; 20 mM Tris-HCl, PH7.5; 150 mM NaCl; 1 mM phenylmethylsulfonyl floride; 1 μg/ml leupeptin). Proteins were separated by sodium dodecyl sulfate-polyacrylamide gel electrophoresis and transferred to PROTRAN BA85 membrane (Schleicher and Schuell, Dassel, Germany). Membranes were blocked with 5% non-fat milk in TBS-T (0.1% Tween-20) and hybridized with anti-FLAG M2 antibody (Sigma), anti-RUNX1 rabbit polyclonal antibody (gift from H Harada) or anti-α-tubulin monoclonal antibody (Sigma) followed by a horseradish peroxidase-conjugated anti-mouse or anti-rabbit immunoglobulin G secondary antibody (GE Healthcare, Pittsburgh, PA, USA). Bound antibodies were detected by enhanced chemiluminescence (GE Healthcare).

Statistical analysis

All statistical analyses were performed using unpaired Student's *t*-test. *P*-values < 0.05 were considered statistically significant.

RESULTS

Derivation of iPSCs from patients with FPD/AML

In order to investigate the physiological function of *RUNX1* in human hematopoiesis and the pathophysiology of FPD/AML, we derived iPSCs from three distinct FPD/AML pedigrees to examine their defects in the emergence of blood cells and hematopoietic differentiation. Three FPD/AML pedigrees that we utilized in the study are depicted in Figure 1a. These pedigrees carried distinct heterozygous mutations in *RUNX1* gene, two in the N-terminal RUNT domain and one in the C-terminal region (Figure 1b). N-terminal mutations in RUNT domain in pedigrees 1 and 2 (G172E and G143W) were considered to affect DNA-binding activity of RUNX1, and C-terminal mutation in pedigree 3 (N233fsX283) was reported to abrogate the transactivation/ repression capacity.

After obtaining informed consent from the affected patients, we established iPSCs from their peripheral T cells by infecting Sendai viruses expressing four reprogramming factors (*OCT3/4*, *SOX2*, *KLF4* and *c-MYC*) (Figure 2a).[34] FPD-iPSCs could be established in comparable frequency as the one from normal individuals (WT-iPSCs), and their behavior in the culture and the morphology of the colonies were indistinguishable from those of WT-iPSCs (Figure 2b). We confirmed that each iPSCs harbored the same *RUNX1* mutation identified in somatic cells of the original patients (Figure 2c). Initial characterization of FPD-iPSCs revealed that the established clones retained typical characteristics of pluripotent stem cells such as the expression of immature ES cell markers (for example, Nanog, Oct3/4, SSEA-3, SSEA-4, Tra-1-60 or Tra-1-81) as examined by immunostaining (Figure 2d), RT-PCR (Figure 2e), qRT-PCR (Supplementary Figure S1a) or flow cytometry (Supplementary Figure S1b) and the ability to form teratomas with differentiation to three germ layers in immunodeficient mice (Figure 2f). Sendai virus-induced reprogramming does not accompany viral integration into the host genome, and we confirmed that the transduced genes were not expressed on mRNA level in the established FPD-iPSC clones (Figure 2e).

Defective emergence of hematopoietic progenitors from FPD-iPSCs

To investigate the impact of *RUNX1* mutation on the emergence of hematopoietic progenitors (HPCs), we induced hematopoietic differentiation of FPD-iPSCs by co-culture on AGM-S3 cells, a stromal cell line established from aorta–gonad–mesonephros (AGM) region[21,35] (Figure 3a). Briefly, WT-iPSCs and FPD-iPSCs were dispersed and plated on inactivated AGM-S3 cells and were co-cultured in the presence of vascular endothelial growth factor.

© 2014 Macmillan Publishers Limited

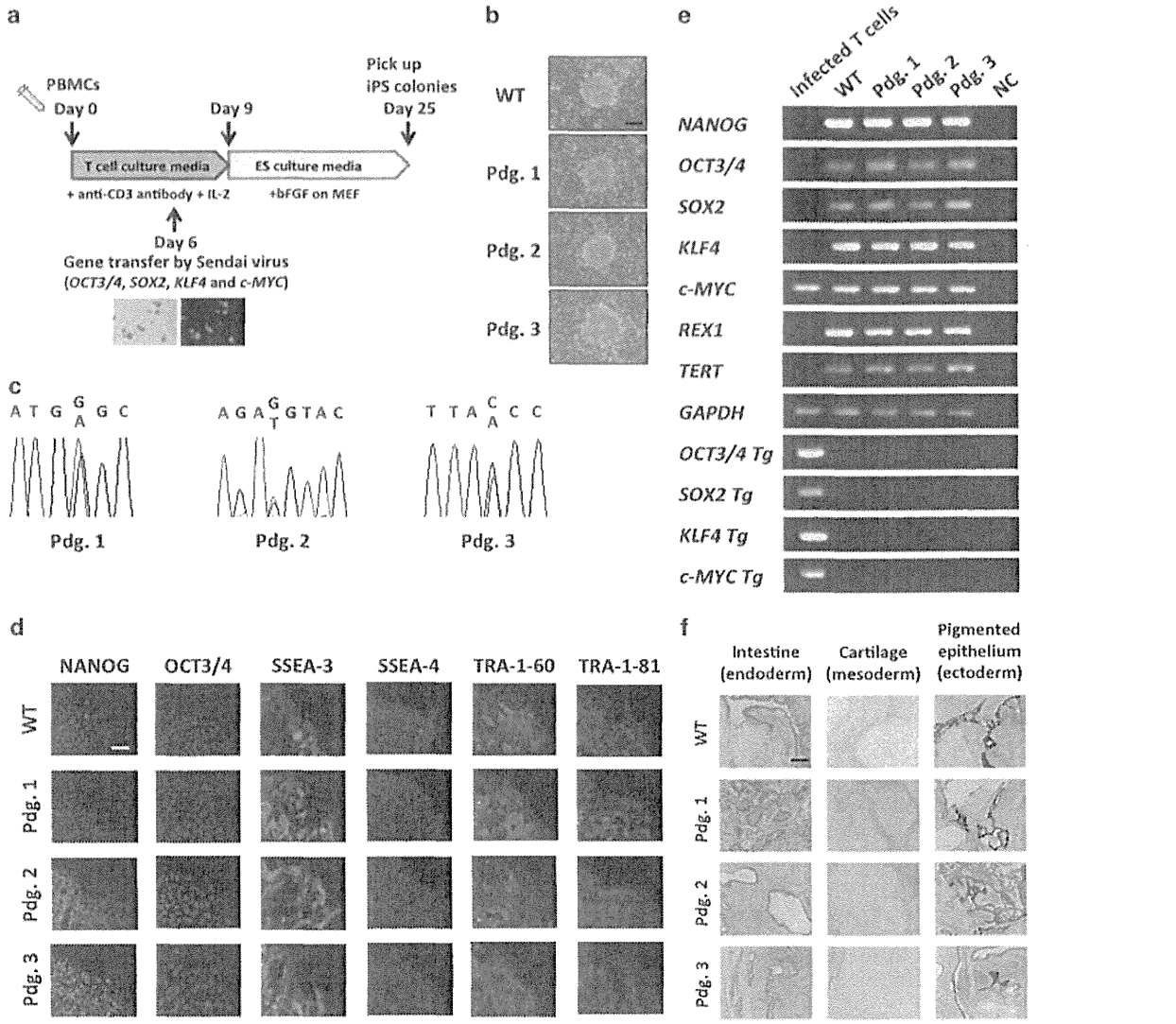

Figure 2. Generation and characterization of iPSCs from FPD/AML patients. (**a**) Schematic diagrams of iPSC derivation from FPD/AML patients using terminally differentiated peripheral T cells. Pictures are T cells infected with control retrovirus expressing green fluorescent protein (GFP) (left; light microscope, right; GFP). (**b**) Morphology of the colonies of WT-iPSCs or FPD-iPSCs. Scale bar = 500 μm. Pdg.; pedigree. (**c**) *RUNX1* mutations in FPD-iPSCs. Each FPD-iPSC retained the same mutation as somatic cells of the original patient. (**d**) Immunofluorescence staining for human embryonic stem cell (hESC) markers. Scale bar = 200 μm. (**e**) RT-PCR analysis for the endogenous hESC maker genes (*NANOG*, *OCT3/4*, *SOX2*, *KLF4*, *c-MYC*, *REX1* and *TERT*), and SeV-transgenes (*OCT3/4 Tg*, *SOX2 Tg*, *KLF4 Tg* and *c-MYC Tg*). NC; negative control. Infected T cells represent T cells 3 days after SeV infection. (**f**) Teratoma formation assay. iPSCs were injected into the testes of NOD-SCID mice. Teratomas were resected, fixed, sectioned and stained with hematoxylin–eosin. WT-iPSC and all FPD-iPSCs showed differentiation to three germ layers, including pigmented epithelium (ectoderm), cartilage (mesoderm) and intestinal glandular structure (endoderm). Scale bar = 50 μm.

On day 15 or day 16 of culture, cells were collected and analyzed for the emergence of HPCs by flow cytometry. Interestingly, the frequencies of $CD34^+$ and $CD45^+$ cells emerged from FPD-iPSCs were decreased to about 40–60% and 20–40% of WT-iPSCs, respectively, suggesting that HPC emergence was profoundly impaired by *RUNX1* mutation (Figures 3b and c). Notably, these defects were observed to a similar extent in all three FPD-iPSC lines, showing that either N-terminal or C-terminal mutations of *RUNX1* do not make any differential effects on the emergence of $CD34^+$ and $CD45^+$ cells. In contrast, expression of CD235a/GPA, an early erthroid-MgK specification marker during human ES cell differentiation,[36] was not impaired in all three FPD-iPSCs as compared with WT (Figure 3c), which suggests that the emergence of early erthroid-MgK progenitors from iPSCs was not affected by *RUNX1* mutation.

In order to quantitatively evaluate the frequency of lineage-committed HPCs derived from each FPD-iPSC, $CD34^+$ cells generated by AGM-S3 co-culture were sorted by flow cytometry and subjected to colony-forming assays. As shown in Figure 3d, the frequencies of granulocyte-monocyte (GM), erythroid (E) or mix colony-forming-cells (CFCs) in $CD34^+$ fraction were significantly lower in FPD-iPSCs as compared with those of WT. It is of note that differences in size and morphology of the colonies were not discernible between WT- and FPD-iPSCs (Supplementary Figure S2).

To examine the HPC emergence in more detail, we undertook ES-sac differentiation protocol to induce hematopoietic differentiation.[32]

© 2014 Macmillan Publishers Limited

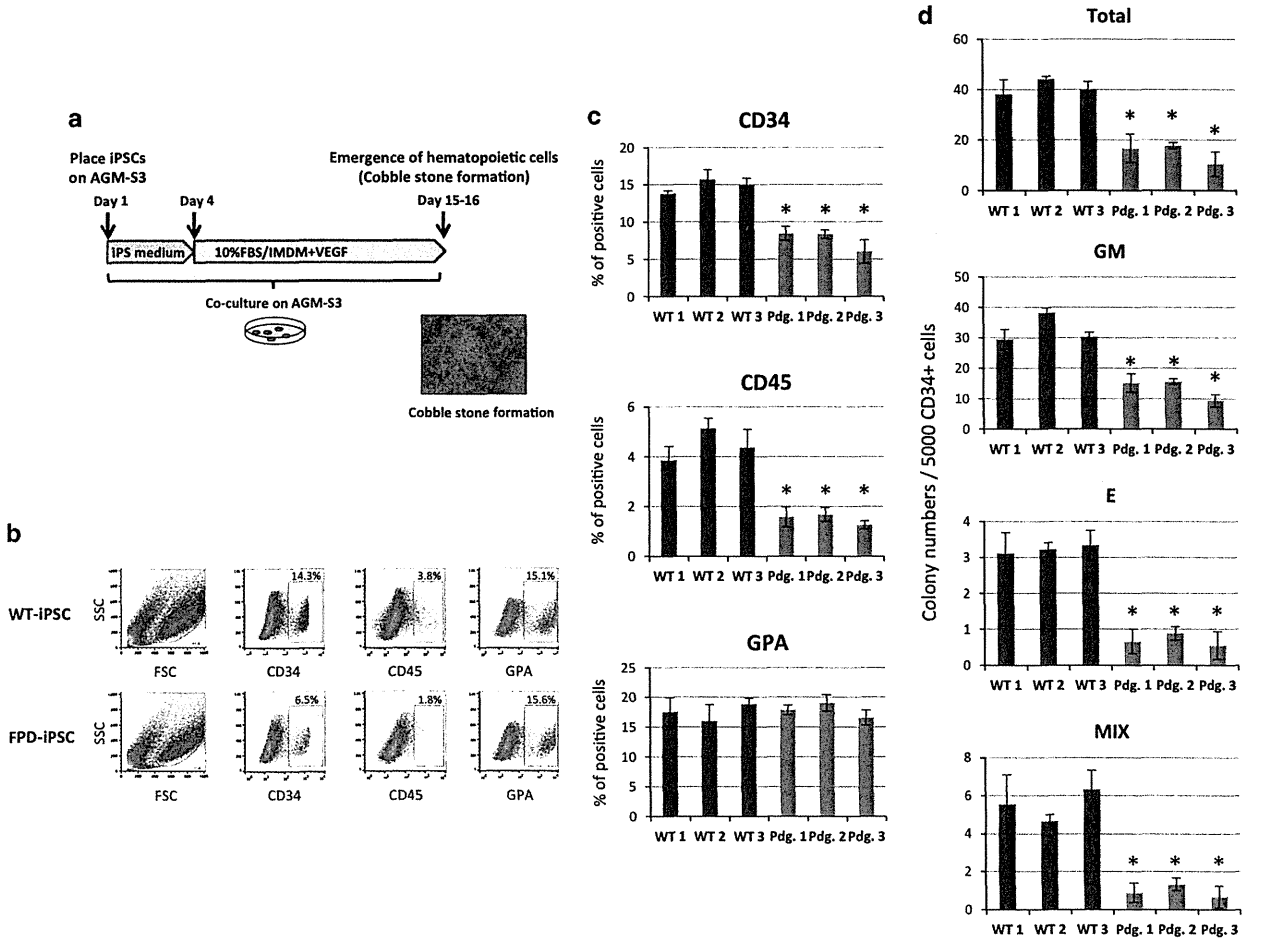

Figure 3. Hematopoietic differentiation of iPSCs by AGM-S3 co-culture. (**a**) Schematic diagram of hematopoietic differentiation of iPSCs by co-culture with AGM-S3. Photograph on the right shows a cobblestone area that appeared around iPSC colonies on day 13. (**b**) Representative flow cytometric profile of cells harvested from AGM-S3 co-cultures. Analyses of WT-iPSC (WT1) and FPD-iPSCs (Pdg. 1) are shown. Mononuclear cell (MNC) fractions were gated and analyzed for CD34, CD45 and GPA. (**c**) Percentages of $CD34^+$, $CD45^+$ or GPA^+ cells against MNCs are shown ($n = 3$, mean ± s.d.). All FPD-iPSCs uniformly showed impaired differentiation to CD34 or CD45 cells, while differentiation of GPA^+ cells remained intact. WT1, WT2 and WT3 represent WT-iPSCs, established from three distinct individuals. *$P < 0.01$. (**d**) Sorted $CD34^+$ cells (5000 cells/ plate) from AGM-S3 co-culture were subjected to colony-forming assay as described in Methods. GM, CFU-GM; E, BFU-E; Mix, CFU-mix. Data are shown as mean ± s.d. ($n = 3$). *$P < 0.01$.

The efficiency of ES-sac induction was comparable between WT- and FPD-iPSCs (Supplementary Figure S3a). As shown in Figures 4a–c and Supplementary Figure 3b, the percentage of $CD34^+CD43^+CD45^-$ cells, earliest HPCs detected during ES cell/iPSC differentiation (HP1), was decreased to 10–40% of WT in FPD-iPSCs.[36,37] Furthermore, $CD34^+CD43^+CD45^+$ or $CD34^-CD43^+CD45^+$ cells, representing late-committed HPCs (HP2) or myeloid-restricted HPCs (Lin P), respectively, were drastically decreased to 3–5% of WT in FPD-iPSCs (Figure 4c). Notably, these frequencies were not statistically different between FPD-iPSCs with N-terminal *RUNX1* mutation (FPD-N-iPSCs) (pedigree 1 and pedigree 2) and those with C-terminal *RUNX1* mutation (FPD-C-iPSCs) (pedigree 3) in this assay. We have also checked the frequency of various lineage-committed progenitors in the fixed number of $CD34^+CD43^+CD45^-$ cells by colony-forming assays. This revealed that the frequencies of GM-, E- and mix-CFCs in $CD34^+CD43^+CD45^-$ cells were comparable between WT- and FPD-iPSCs (Supplementary Figure S3c), and no apparent difference was noted in the morphology of the colonies (Supplementary Figure S3d).

Taken together, these results clearly indicate that the net emergence of HPCs from human iPSCs is profoundly impaired by *RUNX1* mutation.

Defective differentiation and maturation of MgKs from FPD-iPSCs

It has been shown that *RUNX1* was critical for MgK differentiation and maturation by gene-disruption studies in mice.[1] We asked whether this finding could be applied to human settings by using FPD-iPSC-differentiation model. To do this, $CD34^+$ cells induced in AGM-S3 co-culture system were assessed for their ability to differentiate into MgKs in liquid culture with thrombopoietin and SCF (Figure 5a). Interestingly, $CD34^+$ cells from FPD-iPSCs generated $CD41a^+$ MgKs in significantly lower frequencies (30–50%) as compared with WT in this assay (Figures 5b and d). Actual number of MgKs generated from $CD34^+$ cells was also decreased in the FPD-iPSC-group as compared with WT (Supplementary Figure S4). Of note, MgKs differentiated from FPD-iPSCs were less mature and smaller in size as evidenced by CD42b and mean-forward scatter (FSC), respectively, by flow cytometry (Figure 5d). However, differences in size or morphology were not readily apparent by cytospin preparation (Figure 5c).

These results indicate that differentiation of MgKs is impaired both quantitatively and qualitatively in FPD-iPSCs. Again, all three FPD-iPSC lines shared the same phenotype in these assays, suggesting that N-terminal and C-terminal *RUNX1* mutations

© 2014 Macmillan Publishers Limited

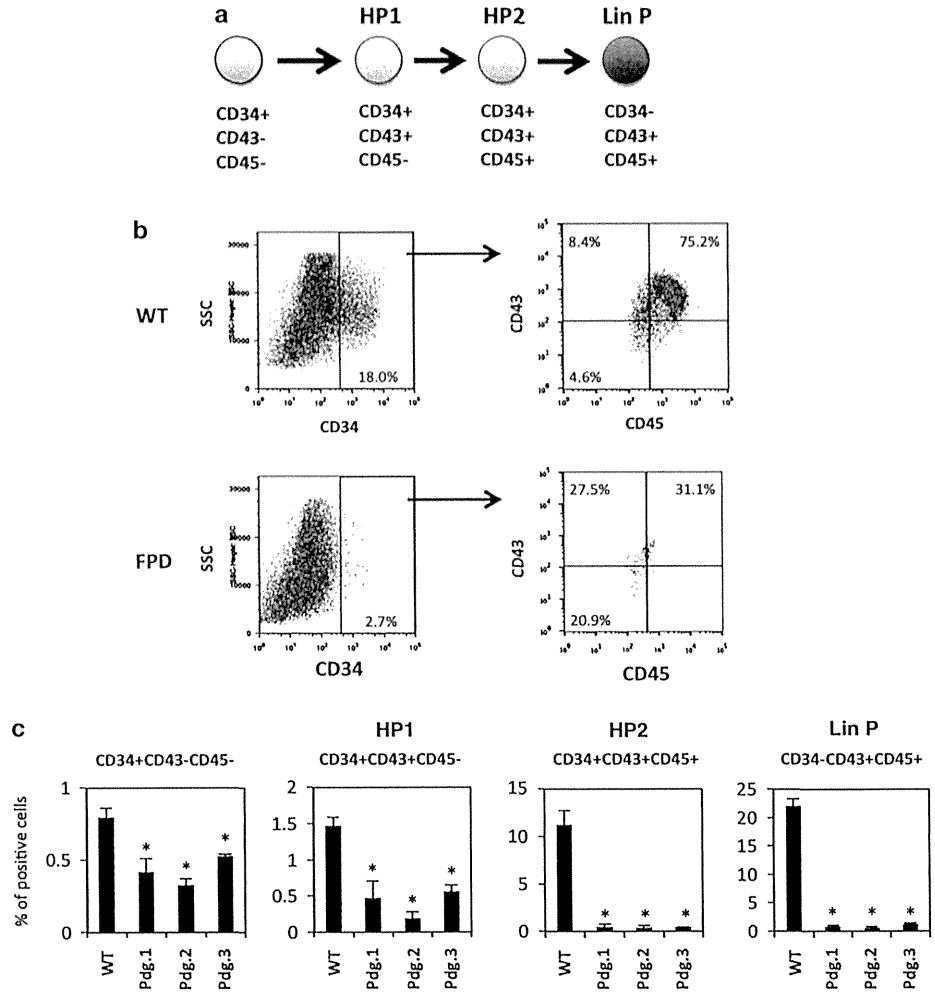

Figure 4. Emergence of hematopoietic progenitors from iPSCs. (**a**) A model of hematopoietic differentiation from human ES cells.[36] HP1, early HPC; HP2, late-committed HPC; Lin P, myeloid-restricted HPC. (**b**) Representative flow cytometric profiles of HPCs generated from WT- or FPD-iPSCs by ES-sac protocol. (**c**) Percentages of HPCs generated from WT- or FPD-iPSCs analyzed by flow cytometry. Data are mean ± s.d. ($n = 3$). $^*P < 0.01$. SSC, side scatter.

impose similar defects in MgK differentiation and maturation in FPD-iPSCs.

Phenotypic rescue of FPD-iPSCs by overexpression of WT *RUNX1*

As mutant *RUNX1* has been reported to act in a loss-of-function or dominant-negative manner for WT-*RUNX1*, we tried to rescue the phenotypes of FPD-iPSCs by overexpressing WT-*RUNX1*. FPD-N-iPSC and FPD-C-iPSC clones (pedigrees 1 and 3) overexpressing WT-*RUNX1* were established by transfecting the vector expressing Flag-tagged WT-*RUNX1*. Three clones for each FPD-iPSC were established, and they presented highly similar phenotype. The expression of Flag-RUNX1 was confirmed by western blotting and RT-PCR (Figures 6a and b). FPD-iPSCs overexpressing Flag-*RUNX1* was morphologically indistinguishable from parental FPD-iPSCs, and their immature phenotype was confirmed by the expression of pluripotent genes such as *NANOG* or *OCT3/4* by RT-PCR (Figure 6b). We then investigated whether these established clones recovered the capacity to differentiate into hematopoietic lineage. As expected, overexpressing WT-*RUNX1* in FPD-iPSCs rescued the emergence of $CD34^+$ and $CD45^+$ cells by AGM-S3 co-culture both in FPD-N-iPSC (pdg. 1) and FPD-C-iPSC (pdg. 3), whereas mock control did not (Figure 6c). Moreover, CFC numbers (CFU-GM, CFU-E, CFU-mix) in $CD34^+$ cells and differentiation of MgKs as examined by CD41a expression and cell numbers were also rescued by WT-*RUNX1* overexpression (Figures 6d and e, Supplementary Figure S5). Morphology of the colonies was not different between parental FPD-iPSC and mock- or Flag-*RUNX1*-transfected FPD-iPSCs (Supplementary Figure S6). Interestingly, however, mean-FSC by flow cytometry was not recovered, and CD42 expression was rescued only in pedigree 3 (Figure 6e). This suggests that overexpression of WT-*RUNX1* only partially rescues Mgk maturation. Of note, RT-PCR analysis showed that the transgene for WT-*RUNX1* was not silenced either before or after the induction of HPCs (Supplementary Figure S7).

Taken together, these results support the notion that mutant *RUNX1* in FPD/AML acts in a loss-of-function or dominant-negative manner to the WT allele in hematopoietic differentiation, although some aspects of impaired Mgk maturation in FPD-iPSCs may not be the consequence of impaired *RUNX1* function.

Expression of RUNX1 target genes in FPD-iPSC-derived HPCs

To obtain clues whether mutant *RUNX1* acts in a loss-of-function or dominant-negative manner in hematopoietic differentiation,

© 2014 Macmillan Publishers Limited

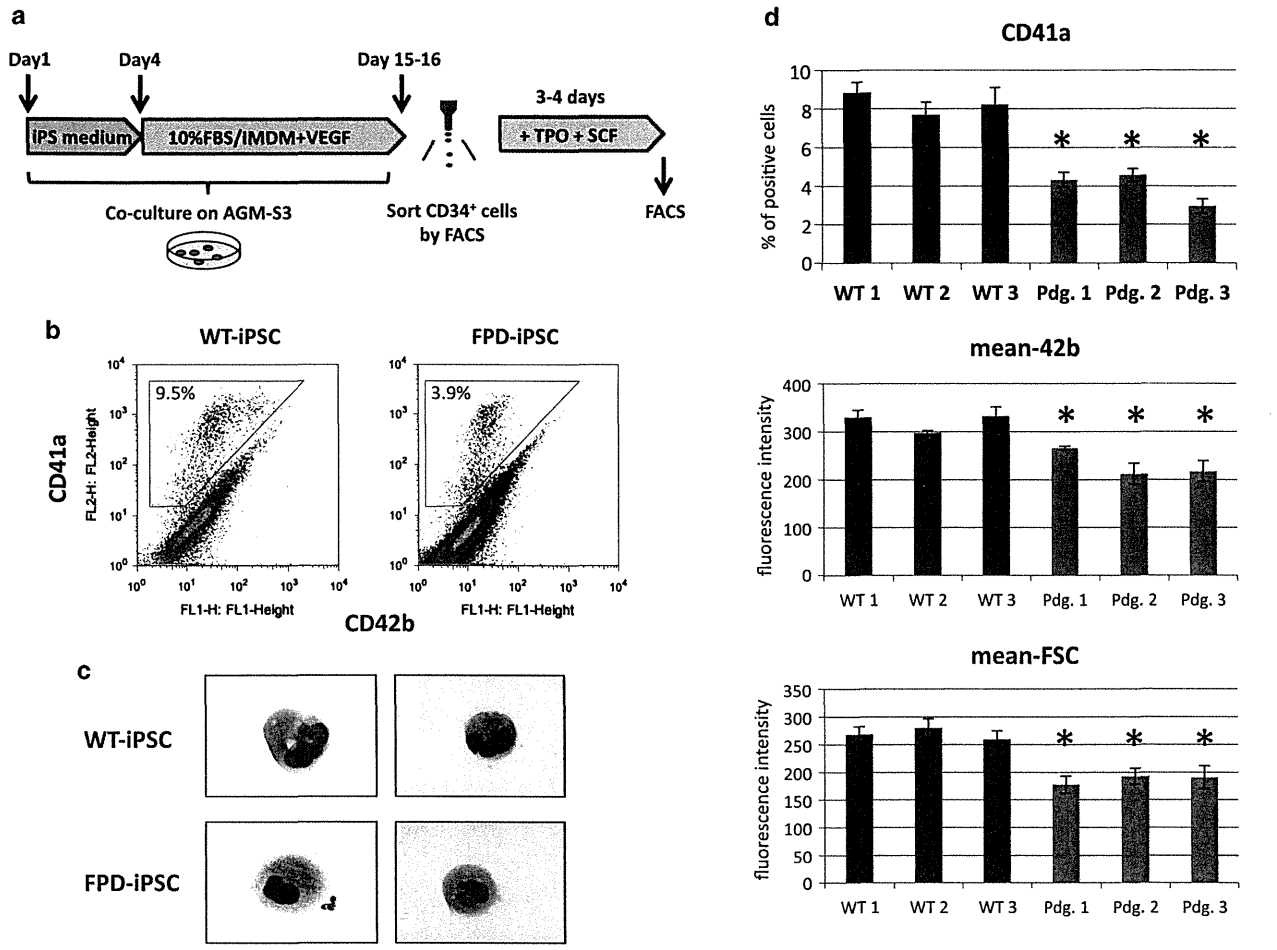

Figure 5. Differentiation of MgKs from iPSC-derived CD34$^+$ cells. (**a**) Schematic diagram of MgK differentiation from iPSC-derived CD34$^+$ cells. CD34$^+$ cells from AGM-S3 co-culture were sorted and cultured in MgK differentiation medium containing thrombopoietin and stem cell factor. Cells were harvested and analyzed on day 3 or 4. (**b**) Representative FACS profile of MgKs generated from iPSC-derived CD34$^+$ cells. Analyses of WT-iPSC (WT1) and FPD-iPSCs (Pdg. 1) are shown. (**c**) Morphology of MgKs derived from WT-iPSC (WT1) and FPD-iPSCs (Pdg. 1) (Giemsa staining. Original magnification; × 1000). (**d**) Percentage of CD41a$^+$ cells, mean fluorescence intensity of CD42b and mean-FSC of WT-iPSC- or FPD-iPSC-derived Mgks are shown. Data are mean ± s.d. ($n = 3$). *$P < 0.01$.

we examined the expression of *RUNX1* target genes by qRT-PCR in hematopoietic cells derived from FPD-iPSCs. Interestingly, expressions of well-known *RUNX1* target genes such as *PU.1*, GM-colony stimulating factor (*GM-CSF*) or myeloperoxidase (*MPO*)[38] in FPD-iPSC-derived hematopoietic cells were decreased to approximately half of those of WT (Figure 7). These data strongly suggest that *RUNX1* alleles of FPD-iPSCs are haploinsufficient.

Overexpression of mutant *RUNX1* in WT-iPSCs does not recapitulate the phenotype of FPD-iPSCs

In order to gain further insight into the role of mutant *RUNX1* in hematopoietic differentiation of iPSCs, we derived WT-iPSCs overexpressing mutant *RUNX1* and examined their differentiation to hematopoietic lineage (Figure 8a). In this experiment, we tested both N-terminal G172E *RUNX1* mutant (*RUNX1*-N^m) from pedigree 1 and C-terminal N233fsX283 *RUNX1* mutant (*RUNX1*-C^m) from pedigree 3.

Three stable iPSC clones for each *RUNX1* mutant were established, and the expression of mutant RUNX1 protein in each clone was confirmed by western blotting (Figure 8a). These clones were then subjected to hematopoietic differentiation assays by AGM-S3 co-culture system. Surprisingly, both *RUNX1* mutants, either *RUNX1*-N^m or *RUNX1*-C^m, scarcely affected the differentiation of WT-iPSCs to HPCs (Figures 8b and c) or MgKs (Figure 8d) as examined by flow cytometry or colony assays, whereas FPD-iPSCs were defective in the same settings (Figures 8b–d). Of note, the expression of mutant *RUNX1* was not silenced in CD34$^+$ cells derived from iPSC clones analyzed (Supplementary Figure S8). These results clearly demonstrated that overexpression of mutant *RUNX1* in WT-iPSCs did not recapitulate the phenotype of FPD-iPSCs. Taken together with the effects of mutant *RUNX1* on the expression of target genes (Figure 7), these results strongly suggest that *RUNX1* mutants act in a loss-of-function, not dominant-negative, manner in hematopoietic differentiation of iPSCs.

DISCUSSION

Knowledge on *RUNX1* function has been mostly derived from genetically modified animals, such as knockout mice or mutant zebrafish. It was previously shown that *Runx1* has a critical role in the establishment of definitive hematopoietic stem cells during embryonic development,[39,40] and the differentiation of MgKs and lymphocytes in adult hematopoiesis.[1] Further studies have shown that *Runx1* was required for the emergence of definitive hematopoietic stem cells from the so-called 'hemogenic

© 2014 Macmillan Publishers Limited

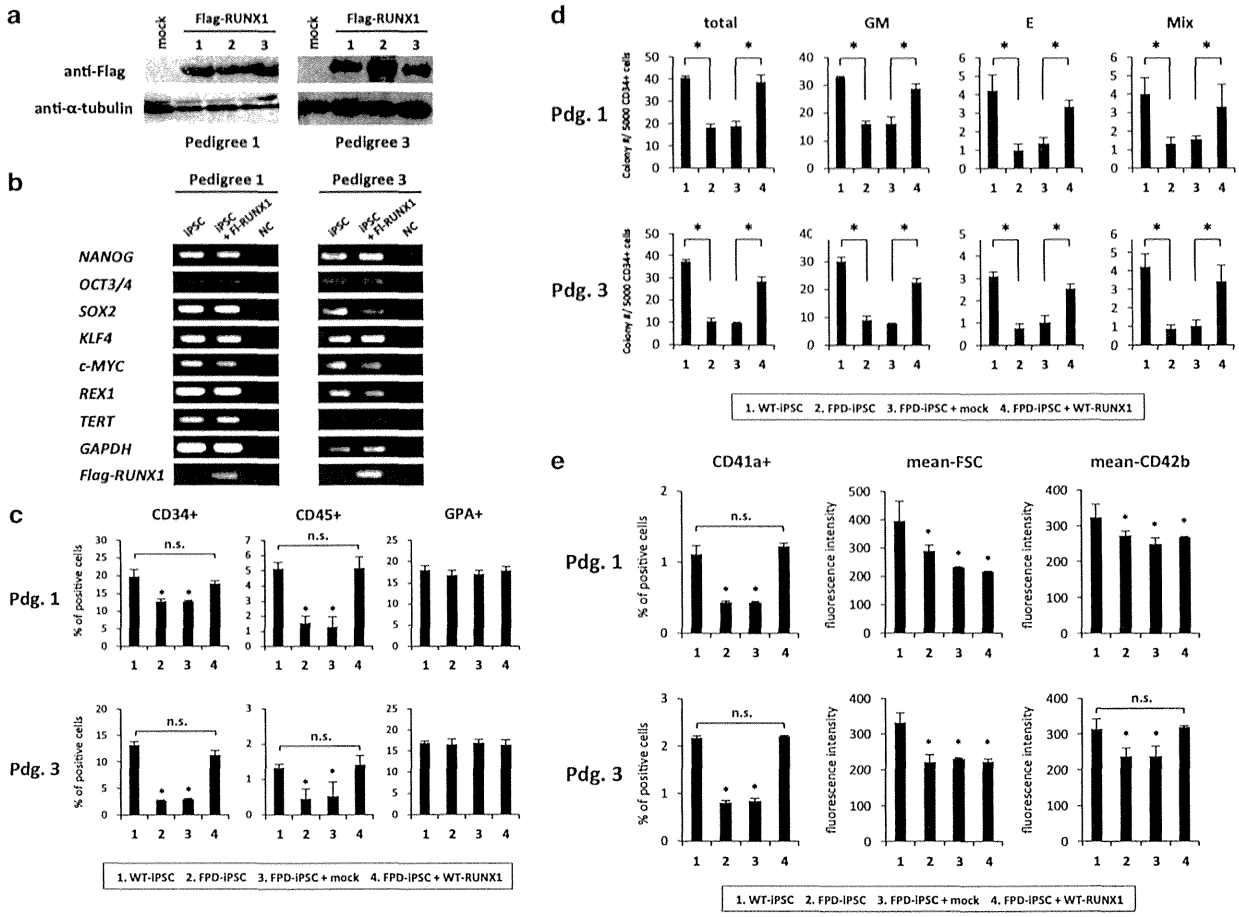

Figure 6. Phenotypic rescue of FPD-iPSCs by WT *RUNX1*. (**a**) Expression of Flag-RUNX1 protein in FPD-iPSCs transfected with pcDNA3/Flag-*RUNX1*. Three different clones were isolated for each FPD-iPSC (pedigrees 1 and 3). The clone numbers are shown on each gel. (**b**) RT-PCR analysis for the endogenous hESC maker genes and Flag-*RUNX1* before and after transfection of Flag-*RUNX1*. Fl-RUNX1, Flag-*RUNX1*; NC, negative control. (**c**) Hematopoietic differentiation of rescued FPD-iPSCs by AGM-S3 co-culture. Percentages of $CD34^+$ cells, $CD45^+$ cells and GPA^+ cells derived from each iPSC are shown. Data are mean ± s.d. ($n=3$). *$P<0.05$. NS, not significant. (**d**) Colony-forming assay of sorted $CD34^+$ cells. Data are mean ± s.d. ($n=3$). *$P<0.05$. GM, CFU-GM; E, BFU-E; Mix, CFU-mix. (**e**) Differentiation of MgKs from rescued FPD-iPSC-derived $CD34^+$ cells. Percentage of $CD41a^+$ cells, mean fluorescence intensity of CD42b and mean-FSC are shown. Data are mean ± s.d. ($n=3$). *$P<0.05$. NS, not significant.

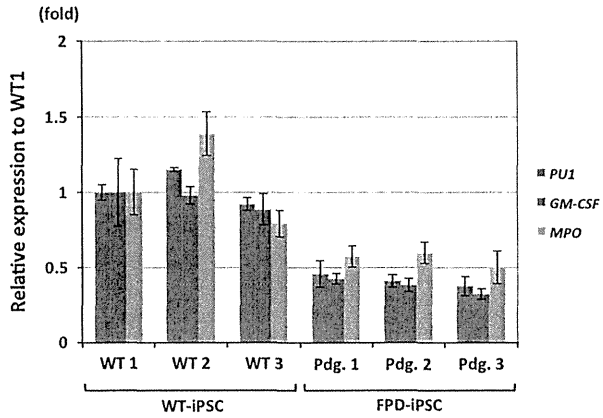

Figure 7. Expression of *RUNX1* target genes in HPCs derived from FPD-iPSCs. Cells recovered from hematopoietic colonies generated from WT- or FPD-iPSCs were subjected to RNA extraction and quantitative RT-PCR analyses for *PU.1*, *GM-CSF* or *MPO*. Data are presented as the relative expression to those of WT1 (mean ± s.d., $n=3$).

endothelium'.[41–44] However, physiological function of *RUNX1* has been rarely investigated in human experimental settings. In order to investigate the impact of *RUNX1* mutation on human hematopoiesis and to delineate the pathophysiology of FPD/AML, we derived iPSCs from FPD/AML patients and examined their defects in hematopoietic differentiation. In this study, we, for the first time, demonstrated that human iPSCs with *RUNX1* mutation are defective in the emergence of HPCs and MgK differentiation.

We also demonstrated that mutant *RUNX1* acts in a loss-of-function manner in hematopoietic differentiation of human iPSCs, strongly suggesting that the phenotypes of FPD-iPSCs are the consequence of haploinsufficiency of *RUNX1*. This is compatible with the previous observation that significant number of FPD/AML pedigrees harbor germline heterozygous deletion of entire or a part of *RUNX1* allele. Furthermore, it was reported that genetically modified mice with heterozygous mutant *RUNX1*-knock-in (KI) alleles, which resembled human hematologic diseases, displayed 60–70% decrease of hematopoietic CFC numbers in AGM regions or FLs during murine embryogenesis, suggesting that they act as haploinsufficient alleles *in vivo*. In contrast, previous *in vitro* biochemical studies have suggested that some of the *RUNX1* mutations observed in MDS or AML act as weak dominant-negative allele.[3,9] They showed that most of the *RUNX1* mutants

© 2014 Macmillan Publishers Limited